AN ABSTRACT OF THE THESIS OF

Erik J. Offner for the degree of Master of Science in Materials Science presented on March 19, 2003.
Title: The Design and Implementation of a Cryogenic Thermal Conductivity Measurement System

Redacted for Privacy

Abstract approved: .....
William H. Warnes

A steady state, axial flow thermal conductivity test apparatus was designed and constructed to operate between room temperature and approximately 4 Kelvin, and to be compatible with existing electronic instrumentation and a continuous flow cryostat. The test design included a radiation shield that had its temperature profile matched to that of the sample to minimize radiation heat transfer losses. The cryostat was used to provide the controllable, low temperature test environment in which the test apparatus would operate. A special wiring bundle was constructed to ensure proper connection of the test device to the required electronic instrumentation, which was controlled from a computer by custom written software. Once assembled, the thermal conductivity of a high purity copper sample was measured over the temperature range from 45 to 300 Kelvin and compared to literature recommended values. The test was performed a second time to check repeatability of the measurements over a range of temperature. Next, the thermal conductivity of a high purity niobium sample was measured and compared to literature recommended values. This test was also performed twice. When completed, these tests had demonstrated the accuracy and repeatability of the measurement of thermal conductivity by the test apparatus over the range of temperatures specified and over a range of conductivities. Finally, the thermal conductivity of a sample of

the bulk metallic glass Vitreloy 1 was measured over the same temperature range. As far as was known, this was the first time the thermal conductivity of this particular material had been tested below 400 Kelvin.

©Copyright by Erik J. Offner
March 19, 2003
All Rights Reserved

The Design and Implementation of a Cryogenic Thermal Conductivity Measurement System

by
Erik J. Offner

A THESIS

submitted to

Oregon State University

in partial fulfillment of
the requirements for the
degree of

Master of Science

Presented March 19, 2003
Commencement June 2003

Master of Science thesis of Erik J. Offner presented on March 19, 2003.

APPROVED:

Redacted for Privacy

Major Professor, representing Materials Science

Redacted for Privacy

Director of the Materials Science Program

Redacted for Privacy

Dean of the Graduate School

I understand that my thesis will become part of the permanent collection of Oregon State University libraries. My signature below authorizes release of my thesis to any reader upon request.

Redacted for Privacy

Erik J. Offner, Author

TABLE OF CONTENTS

TABLE OF CONTENTS (Continued)

LIST OF FIGURES

LIST OF FIGURES (CONTINUED)

LIST OF TABLES

The Design and Implementation of a Cryogenic Thermal Conductivity Measurement System

INTRODUCTION

A number of different properties are used to characterize the behavior of materials. The thermal conductivity is the parameter that characterizes the ability of a material to transfer heat from its hotter to cooler regions. This project was developed from an interest in measuring the thermal conductivity of the bulk metallic glass Vitreloy 1. A system to perform this measurement was not available locally, so a thermal conductivity test system was designed and constructed, tested against known materials, and then used to perform the measurement on a sample of the metallic glass. As this type of research is basic science into the characterization of a material, special applications for the material may not be apparent until the results of the measurements are known. These measurements also help foster a better understanding of the structure and behavior of the material.

Figure 1 presents the accepted literature thermal conductivity of several materials [1]. These curves were generated by Touloukian by curve fitting vast amounts of experimental data spanning, in the case of some materials, a century of work by researchers. Presented in Table 1 are the number of different data curves experimentally generated by researchers and compiled by Touloukian for each material presented in Fig. 1, the span of years covered by the research, and the expected accuracy of the literature accepted curve. From the figure it is obvious that the thermal conductivity of a material varies both as a function of temperature and as a function of material. Increased alloying of a high purity metal produces a corresponding reduction in the thermal conductivity over the entire temperature range. Most pronounced is the reduction in the peak of the curve, which also shifts to higher temperatures with increased alloying. Also apparent is the fact that a uniform crystal structure has a higher thermal conductivity than the same material

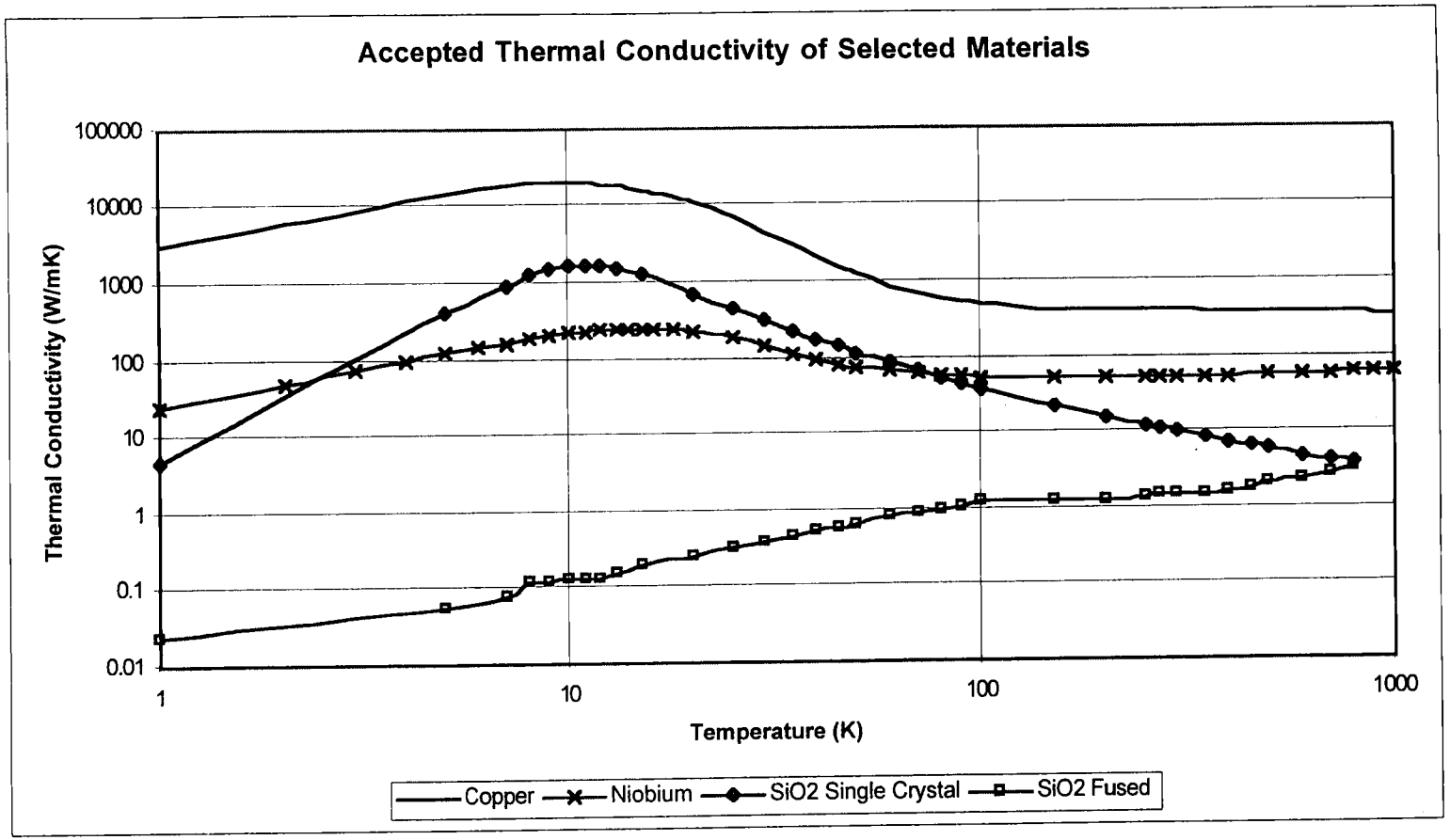

Figure 1. The Accepted [1] Thermal Conductivity of Several Materials.

Table 1. Background and Quantifying Information on the Accepted [1] Thermal Conductivity Curves Presented in Figure 1.

Material	Number of Data Sets Used to Develop the Accepted Curve	Years Spanned by the Research Data Sets	Expected Accuracy Near Room Temperature ± %	Expected Accuracy at Other Temperatures ± %
High Purity Copper	138	1881-1968	3	3-5
High Purity Niobium	51	1950-1966	5	5-10
Amorphous SiO_2	103	1911-1963	5	5-10
Single Crystal SiO_2	71	1884-1958	3	8

in a disordered state, as represented by the non-metallic single crystal and fused SiO_2 curves.

The theory and mechanisms of thermal transport in crystalline materials are considered well understood by researchers. However, the current level of understanding of thermal transport in amorphous, or non-crystalline, materials is at a much less developed state than for crystalline materials [2]. This is particularly true of the recently developed amorphous metals, which are commonly referred to as metallic glasses.

A metallic glass is a metal alloy that has been cooled from the liquid state quick enough that crystallization does not occur, resulting in an amorphous or glassy structure in which there is no long-range order [3]. The critical cooling rate for the early metallic glasses were typically 10^5 to 10^6 K/s to achieve an amorphous solid [4]. To produce a fast enough cooling rate, a melt spinning technique was commonly used in which a molten jet of the alloy would contact the outside diameter of a large, refrigerated, spinning thermal anchor and subsequently produce a ribbon of metallic glass with a maximum thickness of approximately 100μm [3].

Bulk metallic glasses, such as Vitreloy 1 ($Zr_{41.2}Ti_{13.8}Cu_{10.0}Ni_{12.5}Be_{22.5}$), have an increased glass forming ability and corresponding low critical cooling rate of 1 K/s that allows the manufacture of bulk (>1cm) dimension samples through standard casting techniques [4].

Prior to the development of a test device to measure the thermal conductivity of a material, several goals were set to help guide the work. First, to enable the device to test various samples over its lifetime, it had to be relatively easy and inexpensive to change from one sample to another. Next, it was expected that the device would most likely be used to test metal samples, which are generally considered to be good thermal conductors, and so be tailored to suit testing these materials. Finally, the minimization of development expense dictated that the device utilize existing equipment and instrumentation wherever possible. This included a computer and software, electronic control and measurement instrumentation, and a continuous flow cryostat.

A cryostat is a device for producing a controlled low temperature environment in which some other system may operate. It may be a simple container (dewar) to hold a liquid cryogen, which is a substance used for producing very low temperatures, or a more complex device such as used for this application. The continuous flow cryostat employed by this system utilized the continuous flow of a cryogen through a sleeve surrounding the sample space to produce the cold test environment. The temperature of the sample space could be adjusted through regulation of the cryogen flow rate and the application of power to a pair of small electrical resistance heaters in the cryostat. The cryostat was configured to allow the attachment of a vacuum pump to the center bore, or sample space, and its subsequent evacuation. This cryostat center bore is the space into which the thermal conductivity test device would have to fit. The space between the cryogen sleeve and the outer housing of the cryostat contained a radiation shield and was vacuum insulated.

Development of the test device began with a literature review of the various methods of making the thermal conductivity measurement. This was followed by the selection of a particular method that would be compatible with the existing equipment. Next, a study of the related modes of heat transfer and their associated mathematics was performed. Efforts were then made to minimize the heat transfer losses within the selected test configuration. The thermal conductivity test device was then designed for ease of manufacture, to fit the available space, and to allow the use of commonly available fasteners. A three dimensional solid model was then generated to verify the components would assemble correctly and without interference. Next, a series of initial calculations was performed to determine if the expected temperature gradients would be experimentally reasonable and therefore justify construction of the device. Next, the materials and temperature sensors to be used in the construction of the device were selected. Finally, the thermal conductivity test device and associated components were assembled and a series of experiments performed to verify their proper operation.

The completed test system was first used to measure the thermal conductivity of a high purity copper sample at several temperatures covering a range from 45 to 300 Kelvin. The test series was performed a second time to demonstrate the repeatability of the results, which were then compared to the literature accepted [1] values for the material. The same process was performed for a high purity niobium sample to show the device accuracy and repeatability over a range of thermal conductivities. Finally, the thermal conductivity of the bulk metallic glass Vitreloy 1 was measured at several temperatures over the range between 45 and 300 Kelvin. It is believed that this was the first time that the thermal conductivity of this material had been tested below 400 Kelvin.

THEORY

MEASUREMENT METHODS

A tremendous number of different methods for measuring the thermal conductivity of a material have been developed over the years. Much of the variety is due to the different temperature ranges at which the measurement is to be performed and the associated heat transfer considerations, as well as the wide range of thermal conductivity of the various classes of materials to be tested. As such, for a given material and temperature range, one test method may be preferable over the others, but no individual method is suitable for all the potential combinations of test conditions [1]. The primary concern of any of the methods is to achieve a controlled heat flow in the desired direction through the sample so that the theoretical assumptions agree with the actual boundary conditions of the measurement. In general, the various experimental methods of determining the thermal conductivity can be divided into steady-state or nonsteady-state methods.

Steady-state measurement techniques apply a time invariant temperature distribution to the sample and determine the thermal conductivity directly from the temperature gradient and rate of heat flow per unit area. The main steady-state methods are generally classified as either axial-flow or radial-flow. Review of available literature demonstrated that for temperatures below 300 Kelvin, the axial-flow method is used almost exclusively for steady-state thermal conductivity measurements [5].

The axial-flow method of measuring the thermal conductivity uses a system configuration such that the flow of heat is only in the axial direction of the rod or disk shaped sample. Figure 2 illustrates the general arrangement of the axial-flow apparatus. Under steady state conditions it is assumed that the power generated by a heater flows through the sample to a temperature controlled thermal anchor. The temperature difference is then measured over the test length and used to calculate

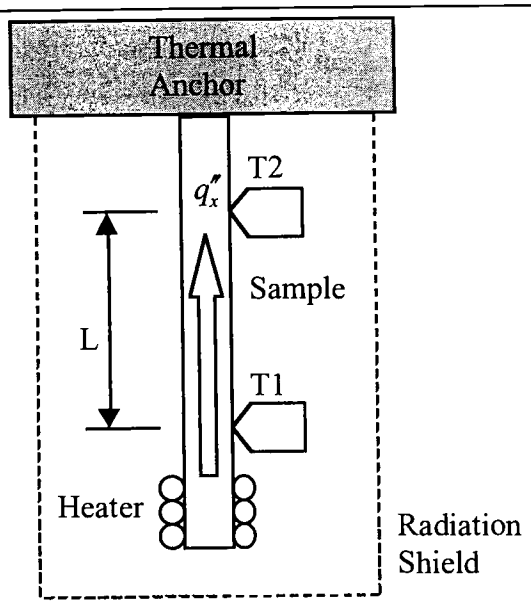

Figure 2. Schematic of Axial-Flow Thermal Conductivity Test Apparatus.

the thermal conductivity of the sample. At cryogenic temperatures, thermal insulation and guard heaters are not normally necessary, but a surrounding radiation shield may be used to minimize the radiation heat loss [1]. For a rod shaped sample, this method is generally considered suitable for good conductors and for all but very high temperatures. A disc shaped sample is suitable for poor conductors.

The radial-flow technique is configured such that the sample heater is enclosed by the sample and the flow of heat is outward through it. There are several variations of this method, such as a cylindrical configuration [6] as shown in Fig. 3, a spherical arrangement, and concentric cylinder and concentric sphere techniques. The concentric techniques contain loose filled sample material between concentric shells and then operate in the same manner as the regular cylindrical or spherical methods.

The nonsteady-state measurement techniques apply a temperature profile to the sample that varies with time. The thermal conductivity of the material is then

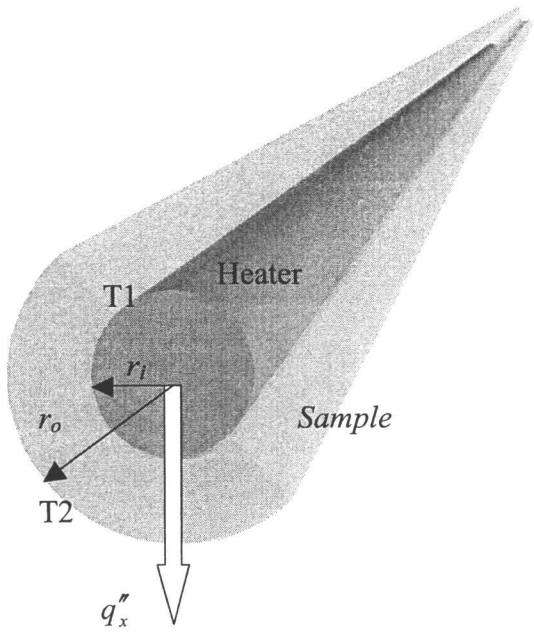

Figure 3. Cylindrical Radial Flow Thermal Conductivity Test Schematic.

calculated from the measurement of the rate of temperature change, which determines the thermal diffusivity, in conjunction with knowledge of the density and specific heat of the sample material. These techniques generally operate using either a periodic or a transient heat flow [1].

TEST METHOD SELECTION

After a review of the most commonly utilized methods of making a thermal conductivity measurement, the variety of instrumentation available in the laboratory and their associated geometric constraints were considered. In particular, the thermal conductivity measurement device had to be configured such that it would be dimensionally compatible with the existing continuous flow cryostat. The cryostat would be used to produce the steady environmental conditions for the test as well as the thermal anchor for the sample. As such, the measurement system had to fit within the limited volume of the cryostat's cylindrical sample space. Of the various techniques, the axial-flow method of

measuring the thermal conductivity was the most compatible with the sample space of the cryostat and was therefore selected for further development. The decision was also made to include a radiation shield in the design of the device, and try to match its temperature profile to that of the sample. An attempt to accomplish this would be made by starting with the general layout of Fig. 2 and attaching a heating element to the end of the radiation shield farthest from the thermal anchor. Next, a temperature sensor would be mounted on the shield at the same axial position as the sample sensor at the T1 location. The power input to the shield heater would be adjusted such that the shield temperature sensor matched the T1 location sample sensor.

HEAT TRANSFER

Prior to designing an instrument to measure the thermal conductivity of a material, all of the various heat flow paths within the system had to be carefully considered. In order to do this the three modes of heat transfer were examined and their effects taken into account during the design. Efforts were then made to minimize these effects on the desired heat flow for the measurement. The transfer of thermal energy occurs through the processes of convection, conduction, and radiation.

Convection

Convective heat transfer is actually a combination of two mechanisms. Thermal energy is transferred by random molecular motion within a fluid as well as by the macroscopic motion of the fluid itself. The mechanism responsible for the fluid motion is generally used to classify the type of convection as forced, such as by a fan or wind, or else as free convection. Free convection is induced by the natural buoyancy forces that develop within the fluid as a result of density differences that are caused by temperature variations [7]. Regardless of the flow type, the convection heat transfer rate equation is given as

$$q'' = h(T_s - T_\infty) \tag{1}$$

and is known as Newton's law of cooling. This equation states that the convective heat flux, q'', is proportional to the difference between the surface at temperature T_s and the surrounding liquid at temperature T_∞. The constant of proportionality, h, is called the convection heat transfer coefficient.

Conduction

The process of conduction heat transfer occurs when thermal energy is transported through a material and the rate of energy transferred per unit of time is known as Fourier's law. This law is not a derivation from first principles but is instead a generalization based on vast experimental evidence and is given as

$$q_x'' = -k\frac{\partial T}{\partial x} \qquad q_y'' = -k\frac{\partial T}{\partial y} \qquad q_z'' = -k\frac{\partial T}{\partial z} \tag{2}$$

The heat flux q'' is the heat transfer rate per unit area perpendicular to the direction of transfer. It is proportional to the temperature gradient along this direction through the thermal conductivity k, a transport property of the material the heat is flowing through. The minus sign in the equation is due to the fact that the heat flows in the direction of decreasing temperature. The heat rate due to conduction is then the product of the flux and the area

$$q_x = q_x'' \cdot A \tag{3}$$

for heat flow through a material of area A. For a one-dimensional system operating under steady state conditions, Eq. 2 and Eq. 3 can be combined and then simplified for the conduction heat rate as

$$q_x = -kA\frac{dT}{dx} \tag{4}$$

For the linear temperature profile and steady state conditions of Fig. 4, the temperature gradient can be expressed as

$$\frac{dT}{dx} = \frac{T_2 - T_1}{L} \tag{5}$$

and when substituted into Eq. 4 the conduction heat rate becomes the easily utilized experimental equation

$$q_x = kA\frac{T_1 - T_2}{L} = kA\frac{\Delta T}{L} \tag{6}$$

From Eq. 2, the thermal conductivity k is defined as

$$k \equiv -\frac{q_x''}{(\partial T/\ \partial x)} \tag{7}$$

Utilizing the previously discussed simplifications for the case shown in Fig. 4 allows this definition to be rearranged into an experimentally useful method for determining the thermal conductivity of a material as

$$k = \frac{q_x L}{A\Delta T} \tag{8}$$

Assuming the utilization of an electrical resistance element as the heat source, the rate of heat input from a direct current power supply was represented by the heater power, P, defined as

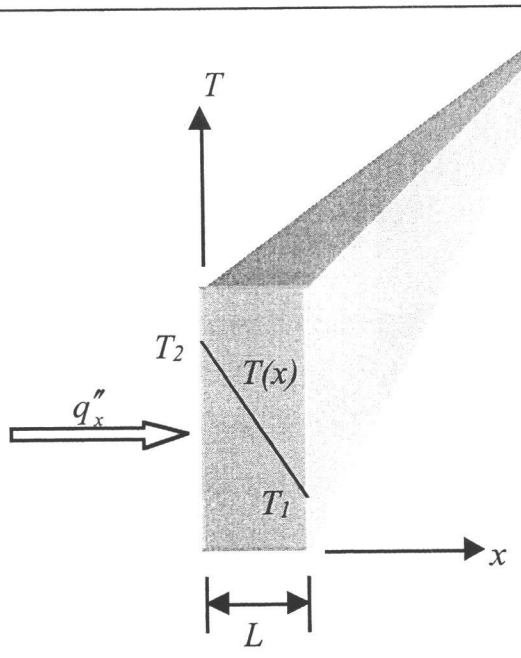

Figure 4. One-dimensional Conduction Heat Transfer Model.

$$P = VI = I^2R \tag{9}$$

In this equation, V is the voltage, I is the electrical current, and R is the electrical resistance. Substitution of the heater power for the heat rate in Eq. 8 yielded the form of the equation used in the experimental determination of the thermal conductivity of the material sample, given as

$$k = \frac{I^2RL}{A(T_1 - T_2)} \tag{10}$$

Having developed a useable relationship for the thermal conductivity of a material, it was important to consider the conduction transfer mechanism itself. Heat is transported in solid materials through thermally activated lattice vibrations, called phonons, as well as the movement of free electrons within the material. Associated with each of these transport mechanisms is a thermal conductivity. The summation of the lattice thermal conductivity, denoted by k_l, and the electronic thermal conductivity, k_e, yields the overall thermal conductivity of the material [8]. This is given as

$$k = k_l + k_e \tag{11}$$

Typically one transport method or the other will predominate. The regularity of the lattice structure has an important effect on the k_l contribution, such that amorphous materials have a lower thermal conductivity than well-ordered crystalline materials [9] as demonstrated by the SiO_2 curves in Fig. 1. A single crystal material may even have a higher peak thermal conductivity than a polycrystalline high purity metal, as is apparent from comparison of the single crystal SiO_2 and high purity niobium curves in Fig. 1. As the concentration of free electrons increases in a material the relative contribution of k_e to the overall thermal conductivity also increases. In high purity metals k_e is the dominant component, while in impure metals or disordered alloys the two contributions may be comparable. This is due to the reduction in the electron mean free path caused by collisions with impurities. In the case of dielectric materials, commonly referred to as electrical insulators, there are essentially no free electrons, so there is no k_e component and the thermal

conductivity is entirely guided by phonon heat transfer. According to Timmerhaus and Flynn [10], "the disordered dielectrics such as glass and polymeric plastics are the poorest solid conductors of heat."

Because free electrons are also responsible for electrical conduction, a relationship has been developed between the thermal and electrical conductivities. The Wiedemann-Franz-Lorenz law,

$$L = \frac{k}{\mu T} \tag{12}$$

states that the ratio of the thermal (k) and electrical (μ) conductivity is directly proportional to the absolute temperature through the Lorenz number, L, [11]. The theoretical value of L for metals, 2.45×10^{-8} $W\Omega/(K)^2$, is independent of the particular metal and agrees very well with the experimentally determined values of the Lorenz number. At low temperatures, however, this relationship is not valid. At room temperature, the Lorenz number has been experimentally determined for many pure metals and covers a range between 2.2 and 3.0×10^{-8} $W\Omega/(K)^2$ [5]. Because the measurement of the thermal conductivity of a material is quite difficult, it is sometimes approximated from the Wiedemann-Franz-Lorenz law using the more easily measured electrical conductivity.

Radiation

When the free electrons within a material at a finite temperature move, energy is emitted. This emission is referred to as thermal radiation. In this heat transfer mechanism, the presence of a material medium is not required for the transfer of energy because the energy is transported by electromagnetic waves (photons). In fact, radiation heat transfer between surfaces is most efficient in a vacuum [9] due to the lack of intermediate material to emit, absorb, or scatter radiation.

The rate at which energy is emitted per unit area is referred to as the emissive power E. The upper limit to the emissive power is defined by the Stefan-Boltzmann law for an ideal radiator as

$$E_b = \sigma T_s^4 \tag{13}$$

where σ is the Stefan-Boltzmann constant ($\sigma = 5.67\times10^{-8}$ W/m^{2}K^4) and T_s is the absolute temperature of the surface. This ideal radiating surface is referred to as a blackbody.

A real surface does not have as large a heat flux as a blackbody at the same temperature due to a reduction in the efficiency of surface emission. The emissivity, ε, is a radiative property of the surface that gives a measure of the efficiency of emission relative to a blackbody and has values in the range $0 \leq \varepsilon \leq 1$. The resulting equation for the heat flux emitted by a real surface per unit area is then given as

$$E = \varepsilon \sigma T_s^4 \tag{14}$$

Radiation may also be incident on the surface from any of the objects or sources in the surrounding environment. The rate at which all the radiation is incident on the surface per unit area is known as the irradiation G. Some fraction of the irradiation may be absorbed by the surface and therefore increase the overall thermal energy of the material. The rate of absorption of irradiation is given as

$$G_{abs} = \alpha G_b \tag{15}$$

where α is a radiative property of the surface termed the absorptivity and its value lies in the range $0 \leq \alpha \leq 1$. The value of α is dependent on the surface itself as well as on the nature of the irradiation.

In the common case of a small surface at temperature T_s that is completely surrounded by a larger surface at T_{sur}, the irradiation may be approximated by emission from a blackbody at T_{sur}. In this situation,

$$G_b = \sigma T_{sur}^4 \tag{16}$$

Assuming a gray surface ($\alpha = \varepsilon$), the net rate of radiation heat transfer from the surface per unit area is then

$$q'' = \frac{q}{A} = E - G \tag{17}$$

and can be expanded by substitution of Eq. 14, 15, and 16 to yield

$$q'' = \varepsilon E_b - \alpha G = \varepsilon\sigma\left(T_s^4 - T_{sur}^4\right) \tag{18}$$

In the specific case of infinitely long concentric cylinders, the outer cylinder is designated as *b* and completely encloses the inner cylinder *a*. Because the ratio of the surface areas of the cylinders is equal to the ratio of the radii

$$\frac{A_a}{A_b} = \frac{r_a}{r_b} \tag{19}$$

the resulting net radiation heat transfer rate from *a* to *b* is then calculated as

$$q_{ab} = \frac{\sigma A_a\left(T_a^4 - T_b^4\right)}{\frac{1}{\varepsilon_a} + \frac{1-\varepsilon_b}{\varepsilon_b}\left(\frac{r_a}{r_b}\right)} \tag{20}$$

When the radiation transfer occurs between two surfaces and one does not enclose the other, only a fraction of the radiation emitted by surface *a* is intercepted by surface *b*. This fraction is referred to as the view factor F_{ab}. The resulting radiation heat transfer rate from the surface is then

$$q'' = \frac{q}{A} = F_{ab}\varepsilon\sigma\left(T_s^4 - T_{sur}^4\right) \tag{21}$$

per unit area. For the particular instance of a pair of coaxial parallel disks, as shown in Fig. 5 and as may occur at the ends of the concentric cylinders, the view factor is given as

$$F_{ab} = \frac{1}{2}\left\{S - \left[S^2 - 4\left(\frac{r_b}{r_a}\right)^2\right]^{\frac{1}{2}}\right\} \tag{22}$$

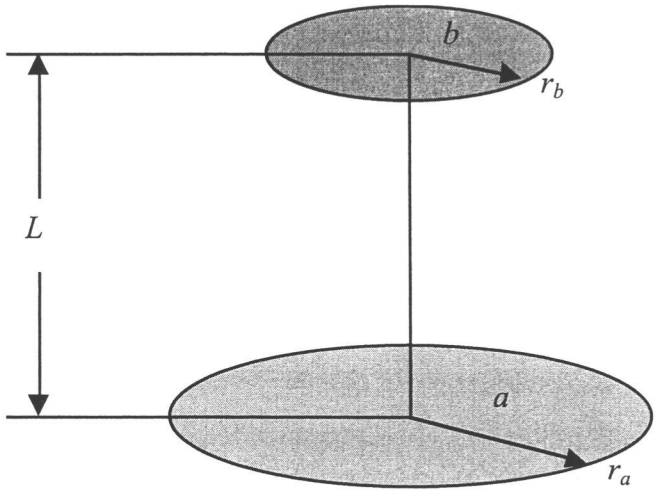

Figure 5. Parallel Disks Model For Radiation Heat Transfer Calculations.

where the value of S is calculated from

$$S = 1 + \frac{1 + \left(r_a / L \right)^2}{\left(r_b / L \right)^2} \tag{23}$$

PROBE DESIGN

Having selected a test technique for measuring the thermal conductivity and developed the associated heat transfer relationships, the specific design considerations were evaluated next. An effort was first made to minimize the heat transfer losses within the test configuration. Next, the specific layout and dimensions of the test apparatus were determined relative to the available space within the cryostat, for ease of manufacture, and to be compatible with the size of commonly available fasteners. A three-dimensional computer model was then generated to verify the correct sizing and relationships between the various components. After the design was complete, a series of initial calculations were performed using the actual dimensions in order to verify that the device would

provide usable temperature gradients. The selection of the particular materials to be used in the construction of the device took place next. With a final computation of the expected component temperatures for the selected materials and geometry, sensors with the required accuracy were chosen. Finally, all of the parts were manufactured, purchased, and assembled.

Minimization of Losses

After the selection of a method for determining the thermal conductivity of a material, the instrumentation and associated components required to actually make the measurement were considered. The configuration of the sensors, their related wiring, and the test environment were carefully considered in terms of the specific thermal flows of the complete system. Efforts were then made to minimize the number and magnitude of heat transfer losses within the theoretical test configuration. Recalling that the primary objective of the thermal conductivity test apparatus is the controlled flow of heat in a particular direction through the material sample, the focus of these minimization efforts was toward losses that diverted heat away from the desired path from the sample heater to the thermal anchor. Losses from the radiation shield and heater to the surrounding cryostat were therefore ignored. Heat flow from the radiation shield and its heater to the sample was, however, considered due to the increase it represented in the actual heat flow along the sample.

Convection

In order to minimize the thermal losses within the system to convection effects, the way in which heat is transferred was more closely examined. From the description of convective heat transfer, transport is dependent on the random molecular motion within a fluid as well as the macroscopic motion of the fluid. The key to convective heat transfer is that both mechanisms require the existence of a fluid, or more specifically for this application a gaseous atmosphere. Elimination

of the atmosphere surrounding the test apparatus also eliminates the convective heat transfer mode.

To remove the gaseous atmosphere surrounding the thermal conductivity test device, a vacuum pump was set to work on the cryostat test space. There was a residual atmosphere due to pumping inefficiencies, but it was so greatly reduced by the vacuum pumping as to render the effect of the convective heat transfer within the system negligible. The remaining atmosphere was further reduced as the temperature within the test space was lowered due to an increasing number of the remaining atmospheric constituents condensing out of their gaseous state. With a continuous reduction of temperature, these constituents eventually froze. The transition from vapor to liquid and then solid resulted in a substantial reduction in volume and therefore a corresponding reduction of the atmospheric pressure. This process is referred to as cryopumping [10,12]. The melting and boiling points of several of these atmospheric constituents are listed in Table 2.

Table 2. The Melting and Boiling Points of Various Atmospheric Constituents [13].

Material	Melting Point (K)	Boiling Point (K)
Water	273.15	373.15
Oxygen	54.75	90.2
Nitrogen	63.29	77.35
Hydrogen	14.01	20.28
Helium	Does not freeze at atmospheric pressure.	4.224

Conduction

Because of the number of physical components required for the construction of the thermal conductivity test device, a large number of potential conductive heat loss pathways exist. The theoretical temperature profile of the sample, considered independently, would develop into isothermal planes perpendicular to the desired axial heat flow through the sample. This would not be the situation near the ends of the sample. Atmospheric conduction from the sample, or conduction from any component attached to the sample, would detract from the desired heat flow from the sample heater to the thermal anchor. The sensors, their method of attachment to the sample, and the sensor lead wires could all produce unwanted heat flow paths. The sample heater lead wires also represented a method of potential conduction heat loss. Finally, the location of the sensors on the length of the sample had to also be carefully considered due to variations in the temperature profile within the sample due to the conduction end effects.

Due to efforts previously undertaken to minimize the convection heat losses, there would be very little or no atmospheric conduction losses either. Because the test space of the cryostat was vacuum pumped, there would only be a greatly reduced atmosphere remaining that would cryopump with decreasing temperature. With the atmosphere removed, the medium for conductive atmospheric heat transfer was also removed.

Several concerns had to be dealt with in regard to the sample sensors. In order to facilitate the desire for easy specimen changes, the sensors needed to be easily separable from the sample. Attachment of the sensors to a device that would then clamp to the sample would allow a solid mounting for the sensor, minimize the risk of damage to the sensor during specimen changes, and provide for a more reproducible mount. This clamp would also provide a place to thermally anchor the section of the lead wires nearest the sensors to ensure that they were at the same temperature as the sensor and clamp.

The sensor clamp needed to have a shape that provided a solid contact to the sample, yet did so over a minimal length of the axis of the sample in order to try to measure the temperature of just one of the isothermal planes. Instead of this ideal, an area contact patch existed as defined by the width of the sample and length of the contact patch along the sample axis. This non-point measurement essentially represented the average temperature over the length of the sample that was in contact with the sensor clamp. The length of surface contact between the sample and the clamp would, however, alter the temperature profile within the sample and therefore result in a deviation from the isothermal planes model in the region of the clamp. Additionally, reduction of the overall size of the sensor clamp would allow the sensor to more rapidly register temperature fluctuations in the sample.

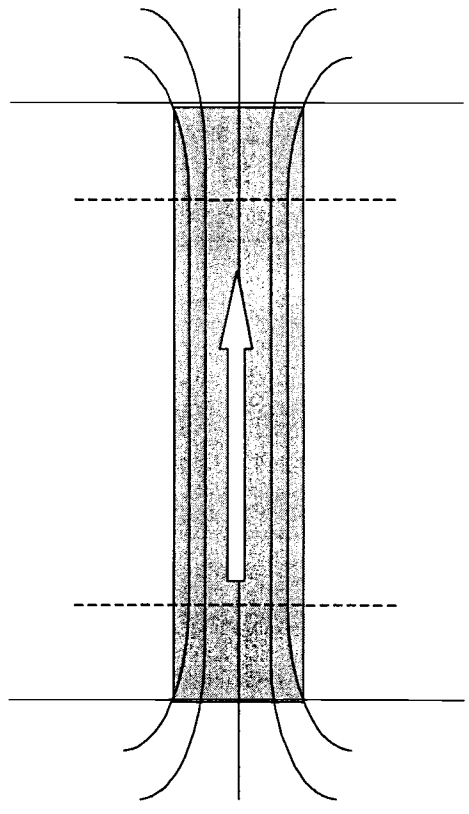

Figure 6. Model of the Heat Flow Through the Sample. Isothermal Planes are Perpendicular to the Flow Lines.

Because the sensor and heater wires eventually connect to the room temperature leads and then to the measuring instruments, the routing of the wires had to be carefully considered. Of particular importance was the path away from the sample sensor and clamp. After leaving the sensors, the lead wires were thermally anchored to the sensor clamp. The sample wiring then ran in a radial direction to the same temperature location on the thermally controlled radiation shield, where the leads were again thermally anchored. Because the wires ran along isothermal planes from the sample to the shield, there was no driving force for conduction heat transfer and therefore no losses along the wires from the sample to the shield. To minimize the thermal conduction losses along the wires themselves for the case where the radiation shield temperature profile did not match that of the sample, small cross-sectional area leads with low thermal conductivities were used.

The final conduction heat transfer consideration that had to be dealt with was the location of the sensors along the length of the sample. The sensors needed to be located far enough from the heater and the thermal anchor to avoid the curvature of the heat flow lines near the sample ends as illustrated by Fig. 6 and in so doing allow the temperature profile within the sample to develop into isothermal planes perpendicular to the desired axial heat flow through the sample. Because of the limited volume within the cryostat sample space, the maximum sample length was physically limited. This also led to a limit on the distance the sensors could be moved away from the sample heater and thermal anchor and still leave a reasonable test length over which the temperature gradient was measured.

Radiation

Elimination of all radiation heat transfer effects within the thermal conductivity test probe was impossible. An effort was, however, made to minimize these losses through the utilization of a radiation shield that surrounds the sample and has its temperature profile matched to that of the sample. Several instruments

were used simultaneously to control the sample and shield heating elements such that the temperature sensors closest to the two heaters, denoted as the T1 location in Fig. 2, were equal. In this manner, the temperature gradient from the sample to the radiation shield in a radial direction was reduced to zero, or very close to it, and the driving force for the radiation heat transfer mode was eliminated or greatly reduced. Additionally, machining the surfaces of the sample and the shield and keeping them clean minimized their emissivities. By inspection of the previously discussed Eq. 20 for the net rate of radiation heat transfer from an inner to an outer concentric cylinder, the reduced emissivities resulted in a corresponding reduction of the rate of heat transfer by the surfaces.

While matching the temperature gradient of the radiation shield to that of the sample resulted in a reduction or elimination of radiation heat transfer in the radial direction, a number of potential radiation pathways still existed. Knowing that the radiation shield and sample were at a higher temperature at the heater end than at the thermal anchor end, some of these remaining pathways were in an axial direction or a combination of axial and radial directions. For example, radiation heat transfer may occur from the sample heater to the slightly cooler sensor clamp, or from a point on the sensor clamp to a lower temperature location on the radiation shield, sample, or even the other sensor clamp. Simple representations of some of these potential radiation pathways are shown by Fig. 7, with the pathway direction down the temperature gradient. Unfortunately, nothing further could be done to minimize these radiation leaks for this particular geometry. The temperature profile matched radiation shield would at least reduce the magnitude of the temperature difference of several of the remaining radiation pathways and subsequently help reduce the rate of radiation heat transfer.

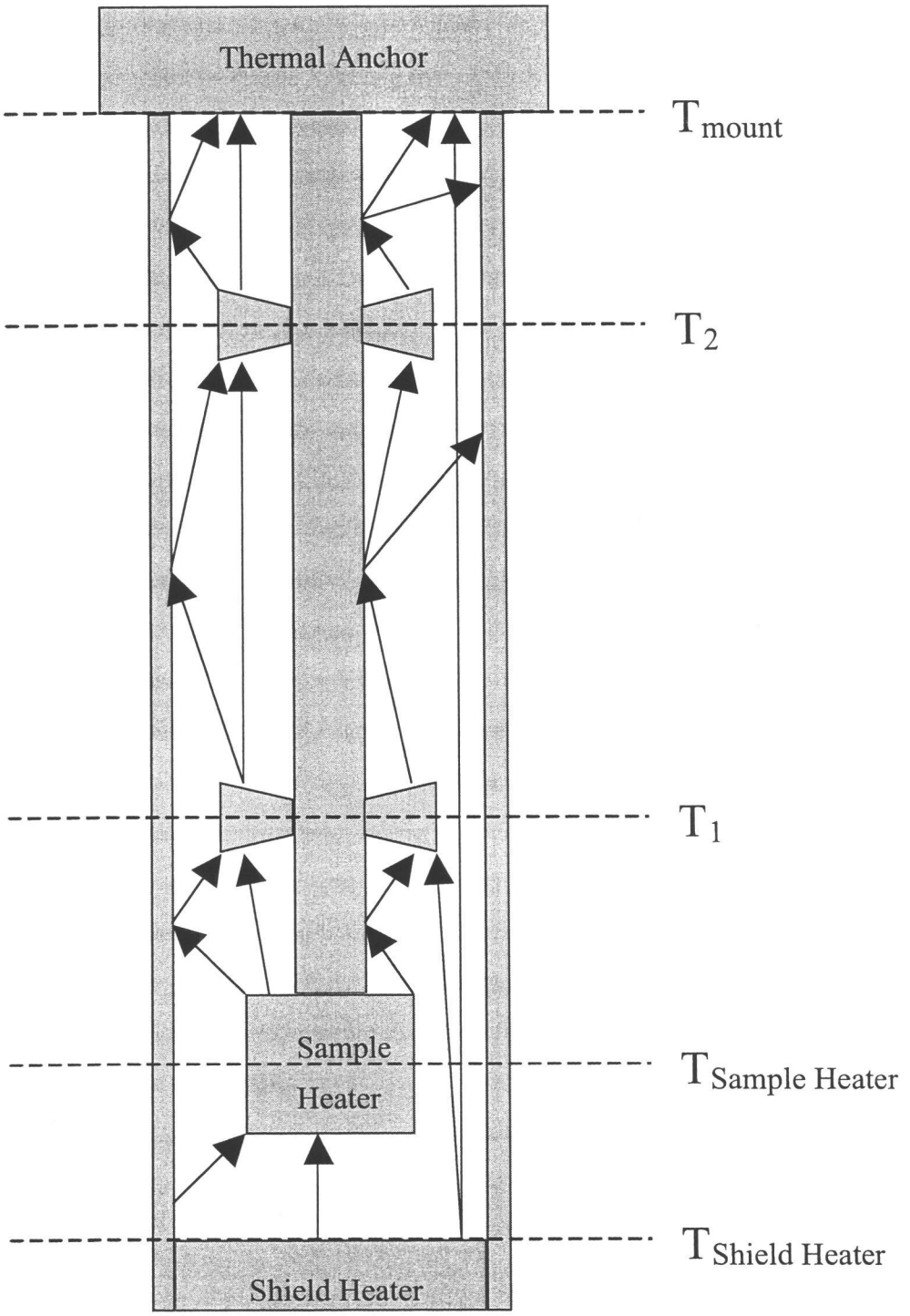

Figure 7. Some of the Potential Radiation Heat Transfer Pathways.

Specific Layout

The basic axial-flow thermal conductivity measurement method from Fig. 2 provided the starting point for the system design. The overall dimensions for this geometry were heavily constrained by the available space within the existing cryostat. As previously discussed, the efforts to minimize the thermal losses within the test system further dictated many of the details of the design, particularly the selection and routing of wiring, sensor location, and sample sensor clamp configuration. The sample itself was designed as a square cross-section bar in order to simplify the design and manufacture of all of the components that mate to it. The cross-section was then made just small enough to allow space for the other system components, but kept as large as possible to reduce the uncertainty/measurement ratio of the area in the calculation of the thermal conductivity.

The individual components to be manufactured were simplified as much as possible in order to reduce the number and complexity of the machining and fixturing steps required for their manufacture. Component shapes were designed so that standard drill and milling machine cutter sizes could be used everywhere possible. The availability of commercially available fasteners further guided the design. The dimensions and sizing information on the drills, mills, and available fasteners in the size range needed for this application were found in the 25th edition of the Machinery's Handbook [14].

With the majority of the design layout completed, a full three-dimensional model was generated to verify that all of the commercially available fasteners and components to be manufactured would fit together properly and with acceptable clearances where needed. This three-dimensional model was generated using Parametric Technology Corporation's Pro/ENGINEER® 2001 solid modeling software and an image of the model is shown in Fig. 8 with the upper shield half removed to better show the inner components.

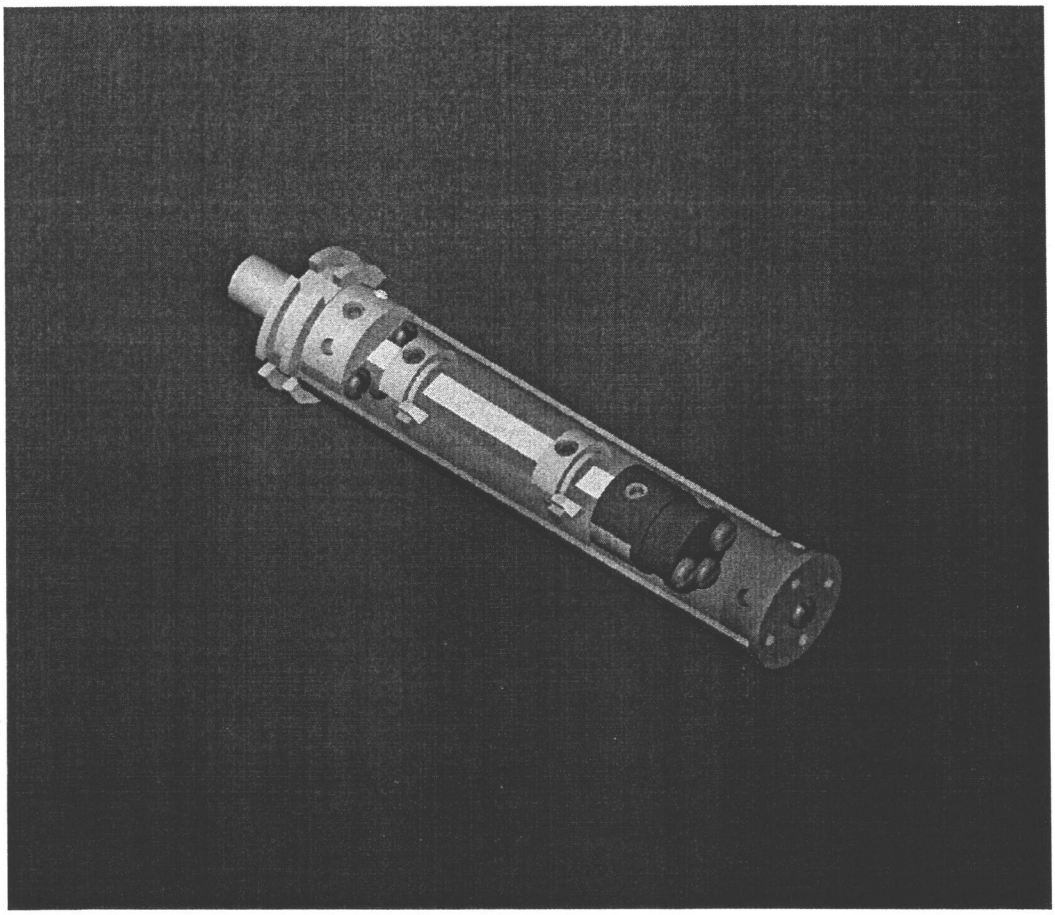

Figure 8. Computer Generated Solid Model of the Thermal Conductivity Test Device. The Upper Shield Half Has Been Omitted for Clarity.

Initial Calculations

After a test system design was selected and the specific geometry determined for ease of manufacturing, fastener availability, and the allowable sample space in the bore of the cryostat, the basic thermal profile of the sample was calculated. In addition, the difference in the rate of radiation heat transfer was determined in the radial direction for a test configuration with no radiation shield, with a non-thermally controlled shield, and finally with a shield thermally matched to the sample. These calculations were performed to foster a better understanding

of the system and possible component temperatures as well as to determine the scale of the gradients involved and if they would be large enough to measure. For these initial computations, the probe temperatures were determined for the system geometry at an environmental temperature of 100 Kelvin with the assumptions of a high purity copper sample, cartridge brass radiation shield, and one-Watt sample heater power input. Because the sample space was vacuum pumped the convective heat transfer mode was not considered in these calculations.

Conduction

With the assumption that the test system was operated under steady-state conditions, the previously discussed equations for thermal conduction could be utilized to determine the temperature profile of the sample. Using Eq. 6 as a starting point and solving for the temperature difference of the sample over the test length yielded

$$\Delta T = \frac{q_x L}{kA} \tag{24}$$

The test length and the cross sectional area were fixed dimensions (L = 25mm, A = 14.44mm^2), the thermal conductivity was for a high purity copper sample at 100 Kelvin (k = 483 W/mK), and the rate of heat input was the assumed one-Watt. With these assumed materials, dimensions, and system conditions, the expected temperature difference was calculated as approximately 3.6 Kelvin. Although not a particularly large gradient, commercially available temperature sensors would allow the measurement of a gradient of this scale. With the thermal anchor held steady at the assumed 100 Kelvin, and knowing the geometry of the system, the above relationship for the temperature gradient could be utilized to determine the temperatures at specific locations over the length of the sample.

By assuming that the temperature profile of the radiation shield was linear and thermally matched to that of the sample by adjusting the component heating elements, a relationship between the shield and sample heater input power could be

derived. Setting the gradient equation, Eq. 24, for the radiation shield and the sample equal to each other, rearranging, and simplifying, the final relationship was calculated as

$$q_r = \frac{k_r A_r}{k_s A_s} q_s \tag{25}$$

where the *r* subscript refers to the radiation shield, and the *s* subscript refers to the sample.

Radiation

The first calculation performed regarding this mode of heat transfer was the determination of the percent change in the radiation heat transfer rate of a test system by the addition of a radiation shield. The system was initially modeled with the sample as an infinitely long cylinder at a given temperature T_i and surrounded by a coaxial environmental cylinder wall at a uniform temperature T_j, such that the net radiation heat transfer rate from the sample to the surroundings could be calculated from the previously developed Eq. 20. Because the radiation losses were based on the surface area of the sample, a cylindrical sample model was developed with the same surface area as the actual sample's surface area. The actual design varied from the model in that it was of finite length and the model sample was round and of uniform temperature, whereas the real design utilized a square cross section sample with a temperature gradient under steady-state test conditions. The approximations were not perfect, but they did allow a greatly simplified computation to be performed.

If a thin, non-thermally matched radiation shield with low thermal conduction resistance was installed within this same system, the rate of heat transfer from the sample to the environmental cylinder wall could be recalculated. The sample and both sides of the shield were assumed to be freshly machined and have an emissivity equal to the test chamber wall in order to simplify the calculations. An emissivity of 0.10 was used based on comparisons to the

representative values of the total, normal emissivity of a variety of materials under a number of different states of preparation [9]. With these assumptions a new value of the net radiation heat transfer rate from the sample to the surroundings was computed.

The addition of a radiation shield to the test configuration resulted in approximately a 38% reduction in the rate of radiation heat loss from the sample to the environment. If this same radiation shield was also thermally controlled to match the temperature of the sample, then inspection of the radiation equation, Eq. 18, shows that there would be no temperature difference between the components. The lack of a temperature gradient would eliminate the driving force for radiation and thereby reduce the rate of radial heat loss due to radiation effects to zero.

With the temperatures of all of the system locations calculated from the conduction equation and the assumption that over the length of the sample the radiation transfer was only in the radial direction and over a temperature gradient of essentially zero, the radiation from the hotter shield heater to the cooler sample heater was considered. The radiation heat transfer between these two surfaces was modeled by a pair of coaxial parallel disks and therefore used the mathematical relationships developed by Eq. 22 and Eq. 23. After filling in the system dimensions and temperatures determined from the conduction equation for the one-Watt sample heater input, the flow of heat from the radiation shield heater to the sample heater was calculated as only 0.001 Watt. This was only a change in the actual energy flow through the sample of approximately 0.10 percent.

Material Selection

Because this test system was entirely new construction there was tremendous freedom to select materials for use in the fabrication of components. First, a general review of materials and alloys used for low temperatures and their thermal, elastic, and mechanical properties was performed [15]. Next, a closer look at some of the materials commonly used in the construction of cryostats [12,16]

was performed as an example of the material applications. From these literature reviews it became apparent that materials were usually selected for an application based on their thermal, mechanical, magnetic, or corrosion resistance properties.

A relatively small number of different materials are most commonly used in the design and construction of cryogenic equipment. Type 304 stainless steel is commonly used in structural applications because of its low thermal conductivity and good mechanical properties. It is widely available at a moderate price in a variety of forms, has good manufacturing properties and corrosion resistance, and can be processed to provide a low radiation emissivity and vacuum outgassing rate. It is also non-magnetic, a property desirable for superconductivity experiments and other magnetic field testing. Oxygen Free High Conductivity (OFHC) copper is used for heat transfer applications for its extremely high thermal conductivity and ease of processing. Series 6061 aluminum is frequently used for vacuum shells, piping, and heat exchangers because of its good thermal conductivity and strength, low weight, and moderate cost. For glass dewars or other systems where optical access is required, silica glass is commonly used. Grade G10 glass-reinforced plastic is commonly used under tension or compression due to its high ratio of strength to thermal conductivity [15]. While these are the most commonly used materials for cryogenic applications, a variety of other materials may be selected for a particular application based on a material property and its relevance to some specific system conditions. Having developed a better understanding of the materials commonly utilized in the construction of cryogenic equipment, the material selection process began for the components of this design.

The use of high thermal conductivity materials in the construction of the test device would allow the system to respond to environmental changes or variations in heater input more rapidly and therefore achieve an equilibrium, steady state more quickly. The selection of the ideal radiation shield material was complicated by the relationship between the thermal conductivity of the sample and the radiation shield as shown in the previously developed heater input ratio given as

Eq. 25. To gain a better idea of the effect of this relationship on the temperature gradient of the sample, a spreadsheet was developed for predicting the gradient and sensor temperatures under test conditions. The thermal conductivity values of the materials selected for consideration in this design were entered into the spreadsheet at representative environmental test temperatures for various combinations of sample and shield materials. Figure 9 shows the calculated variation in the maximum expected gradient as a function of temperature for a few of the considered shield and sample combinations, while obeying Eq. 25 and not exceeding the one Amp heater output capacity of the available temperature controllers. These computations assumed the highest possible output from each heater while maintaining matching temperature profiles between the shield and sample without exceeding the capacity of the temperature controllers. After inspection of the various gradient plots, brass was selected for use in the construction of the radiation shield due to its good behavior in conjunction with the range of expected thermal conductivity samples.

After deciding which material to use for the manufacture of the radiation shield, a material had to be chosen for use in the construction of the remainder of the probe. A very high thermal conductivity material was desirable for use in the probe components so that they would not limit the overall system thermal

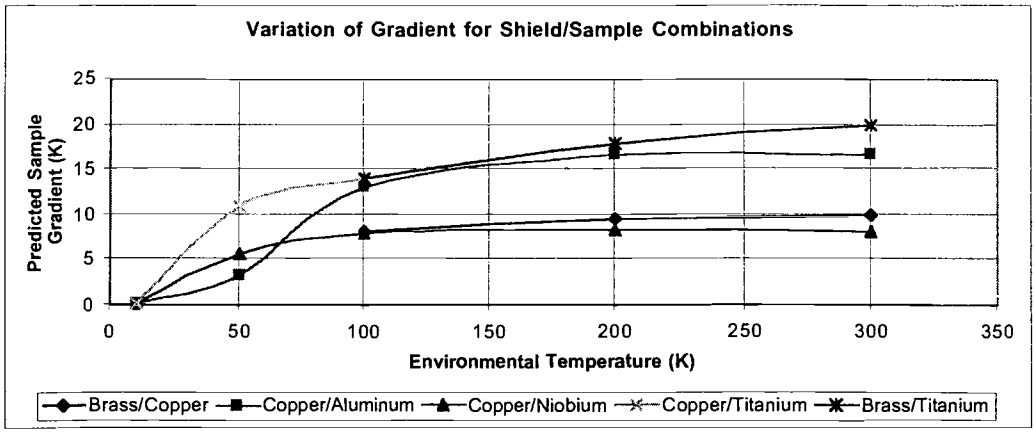

Figure 9. The Maximum Expected Temperature Difference Between the Sample Sensors for Several Shield and Sample Combinations.

conductivity. Among the commonly available materials for use in cryogenic applications, the requirement of a high thermal conductivity quickly narrowed the list of the best options to aluminum and copper. Because most of the probe components had threaded holes and other small features in them, the material to be used in their construction had to be relatively easy to machine, yet sturdy enough not to strip or bend too easily. This final requirement made it obvious that aluminum was the best option for use in the manufacture of the probe components.

Next, the fastener material to be used in the assembly of the thermal conductivity test device was selected. In the fastener sizes required for this design, only a few material types were readily available. Stainless steel fasteners were eventually selected for their availability, non-magnetic properties, and resistance to the condensation-based corrosion that may occur from the numerous thermal cycles the test device would experience.

Finally, the particular material to be used in the construction of the heating elements had to be selected. Based on the geometry developed previously to satisfy the heat transfer, available space, and manufacturing requirements, the remaining space for the heating elements was quite limited. Using the dimensions of the heating element grooves from the design, as well as the diameter of the more commonly used heater wire, the approximate length of wire that could fit into the grooves was computed for an ideal packing configuration. Due to the likely packing gaps, the actual length of wire that would fit the available space would only be a fraction of the ideal, for a final wire length of approximately 75-centimeters. The specifications on the temperature controllers available in the laboratory are stated to produce maximum power when used in conjunction with a heater of 25 Ω resistance. Of the commercially manufactured, commonly available wire types, Nichrome (Ni-20%Cr) heater wire was the only one that provided the desired 25 Ω resistance over the 75-centimeter length. As such, Nichrome wire was selected for use in the construction of the heating elements. Phosphor bronze wire was chosen for the electrical leads from the heaters because its lower electrical

resistance would more efficiently pass the heater current and therefore not create as much electrical heating in the rest of the heater circuit. Additionally, phosphor bronze has a low thermal conductivity and would therefore limit the heat leak into the low temperature test environment.

Sensor Selection

After the selection of the materials to be used for the construction of the test probe, and considering the thermal conductivity range of the anticipated test materials, the expected probe temperatures and gradient were recalculated. Inspection of the plot of the maximum possible gradient as a function of temperature for the selected materials showed a general increase in possible gradient with increasing environmental temperature. As such, at low environmental temperatures there was a very small gradient and therefore a need for the highest resolution sensors available to fit the geometry. The primary means of measuring temperature in cryogenic applications are by diode, thermocouple, and resistance thermometry [15].

To reduce the financial expenditure required for the construction of the thermal conductivity test apparatus, the temperature sensors used on the device had to be compatible with the existing laboratory instrumentation from Lake Shore Cryotronics. The laboratory was equipped to monitor thermocouples, three silicon diode sensors, or a single Resistance Temperature Device (RTD). This design required the use of four sensors, however. All of the mentioned temperature sensor types had models available that covered the desired temperature range, but the diode and RTD sensors were more accurate at lower temperatures than the thermocouples. By selecting silicon diodes over RTD's for this application, only one additional circuit board needed to be purchased for the preexisting temperature controller.

The physical geometry that was developed to be compatible with the cryostat geometry, manufacturing concerns, available fasteners, and heat transfer

considerations left minimal space to accommodate the sensors. A number of silicon diode sensor packaging options were available, but the geometric constraints limited the options to either a bare sensor or the smallest available sealed package. Due to its more rugged nature, the sealed SD package was selected in a four-lead configuration in order to isolate the voltage and current leads. The wires were arranged as a twisted pair of twisted pairs in order to minimize induced currents in the wires as a result of noise pick-up from stray magnetic fields in the research laboratory.

Because of the reduction in temperature gradient with decreasing environmental temperature, the accuracy of the sensors was carefully considered. To reduce the uncertainty in the temperature gradient, and subsequently the uncertainty in the calculation of the thermal conductivity of the material, the sensors had to be as accurate as possible. As such, the SD package silicon diode sensors were fully calibrated by Lake Shore at the time of purchase.

SYSTEM CONSTRUCTION

After completion of the design of the thermal conductivity test device and solid modeling using Parametric Technology Corporation's Pro/ENGINEER® 2001 software, detailed manufacturing drawings were generated. These drawings were then given to the Oregon State University Mechanical Engineering department's machine shop. Student employees of the shop then proceeded to manufacture the radiation shield halves, sensor clamps, and all of the other required components. While the custom components were being machined, the wires, sensors and additional circuit board were ordered and all of the necessary fasteners purchased.

After all of the required components were gathered together, the assembly process was begun. First, a trial assembly was performed of the parts manufactured by the machine shop to verify the correct fit of each of the components. Edges were rounded along the sensor and heater wire routing paths to reduce the chance

of wire insulation damage and subsequent electrical shorting. Once satisfied with the state of each component, the system was disassembled and each fastener and machined part thoroughly cleaned with methanol. The mating surfaces of each part were then coated in a thin film of Apiezon®-N thermal grease to enhance the thermal contact between the components. The pieces were then carefully assembled and the fasteners tightened. Once the solid structure of the test device was put together with an aluminum assembly sample blank, the installation of the electronic instrumentation began.

Each of the heating elements was constructed from an approximately 75-centimeter section of Nichrome heater wire. The wire length was folded in half and twisted at approximately 1.5 twists per centimeter so that the opposing direction of current flow in each half would also create a magnetic field to cancel that generated by the other. The twisted heater wire was then wound into the machined groove on the appropriate components. After a temporary method of securing the wires was devised, a layer of IMI-7031 Insulating Varnish and Adhesive (formerly referred to as GE-7031 varnish) was applied to the heater wire wraps and the heater was then baked at approximately 150°C for 45 minutes to fully cure the varnish. Figure 10 is a digital image of the heater wire installed on the sample heater, which is mounted to the end of the aluminum assembly sample blank. After the Nichrome heater wire was fixed in place with the varnish, phosphor bronze lead wires were attached by soldering and the junction was then insulated with a layer of varnish. In a manner similar to that used in the construction of the heating elements, the silicon diode sensors were installed on the sensor clamps. A thin layer of varnish was applied to the bottom surface of the sensor, which was then carefully held in place by a combination of tools and small weights while the varnish was baked to cure. With the sensors mounted in the correct locations, the wires were routed in short sections along the groove in the circumference of each side of the sensor clamp, temporarily fixed in place through various clamping techniques, varnished, and then baked to cure as for the heating elements. After the allotted time in the

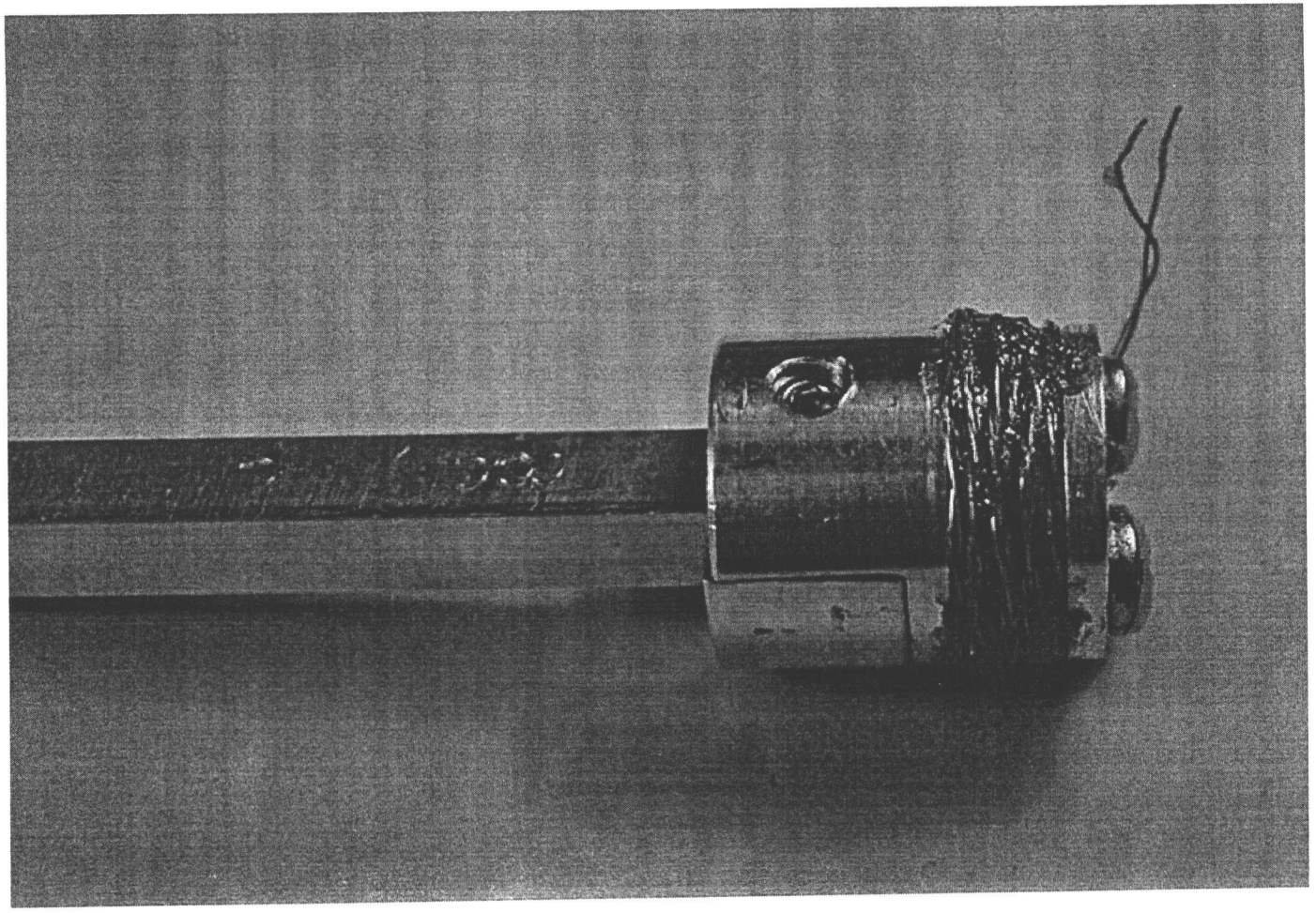

Figure 10. Digital Image of the Nichrome Heater Wire Installed on the Sample Heater Components, Which are Mounted to the Aluminum Assembly Sample Blank.

oven, the pieces were cooled and the process repeated for the next section of wire. Figure 11 shows the temperature sensor wires varnished in place on the sensor clamp with a ruler in the background to provide scale.

The temperature sensors on the radiation shield were attached using the same techniques as were used on the sample sensors and their respective clamps. After the shield sensors were in the correct locations and the varnish was baked to cure, approximately the first two centimeters of wiring from each sensor was thermally anchored along the same isothermal plane of the shield as the sensor. Next, the wiring from the sample sensors and the sample heater were routed radially outward along the isothermal planes to matching temperature locations on

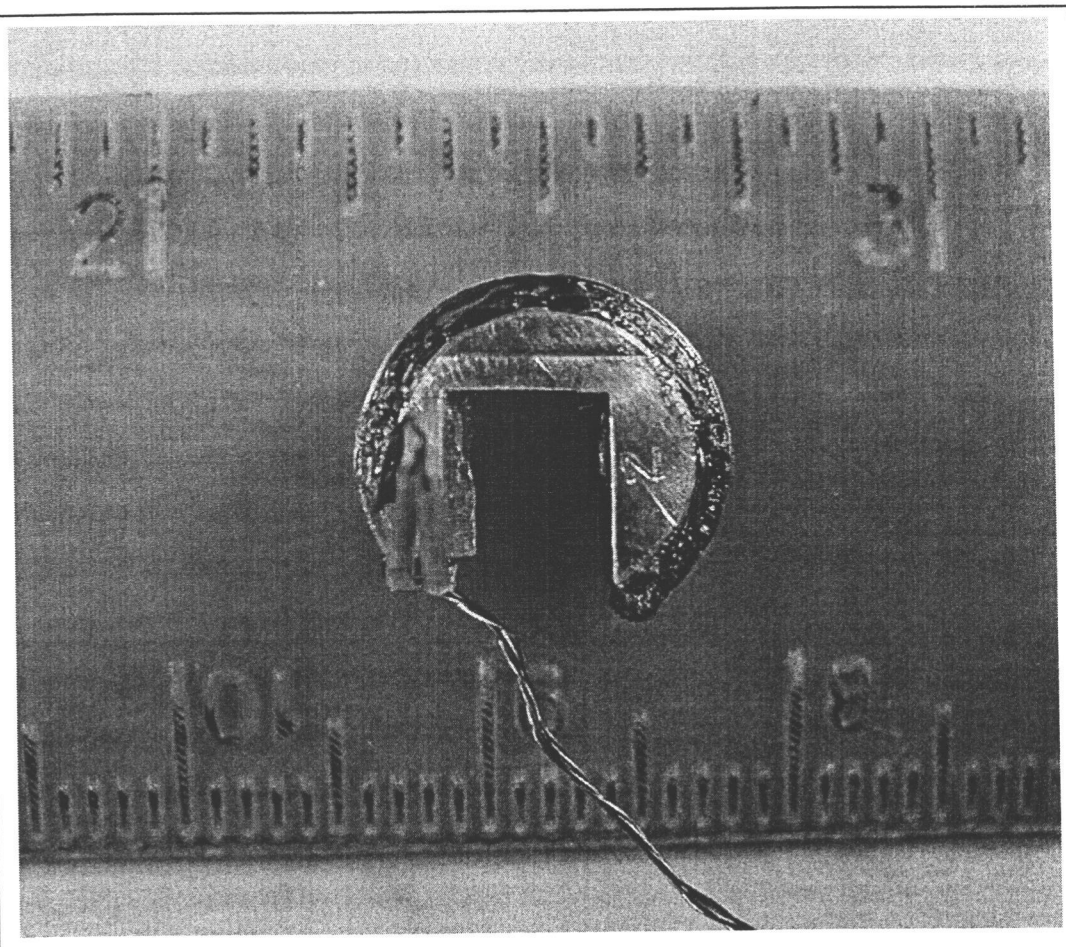

Figure 11. The Sensor Clamp With Wires Varnished in Place.

the radiation shield. Some slack was left in the wires between the sample and the shield to facilitate easier changing of the sample. The configuration of the components and routing of wire from the sample to the radiation shield is shown in Fig. 12. The wires were then thermally anchored over approximately a two-centimeter distance along the same isothermal plane of the radiation shield. Once anchored along the isothermal plane, the wires were then routed axially along the shield toward the main probe thermal anchor with the cryostat inner wall, as shown in Fig. 13. The wires were periodically varnished into place along the shield to prevent them from moving, but still allow for thermal expansion and contraction differences between the wires, shield, and varnish. After all of the sensor and heater wires were gathered together at the probe mount, they were wrapped and varnished into the machined groove of the mount to thermally anchor the wires to the location on the probe closest to the cryostat inner wall.

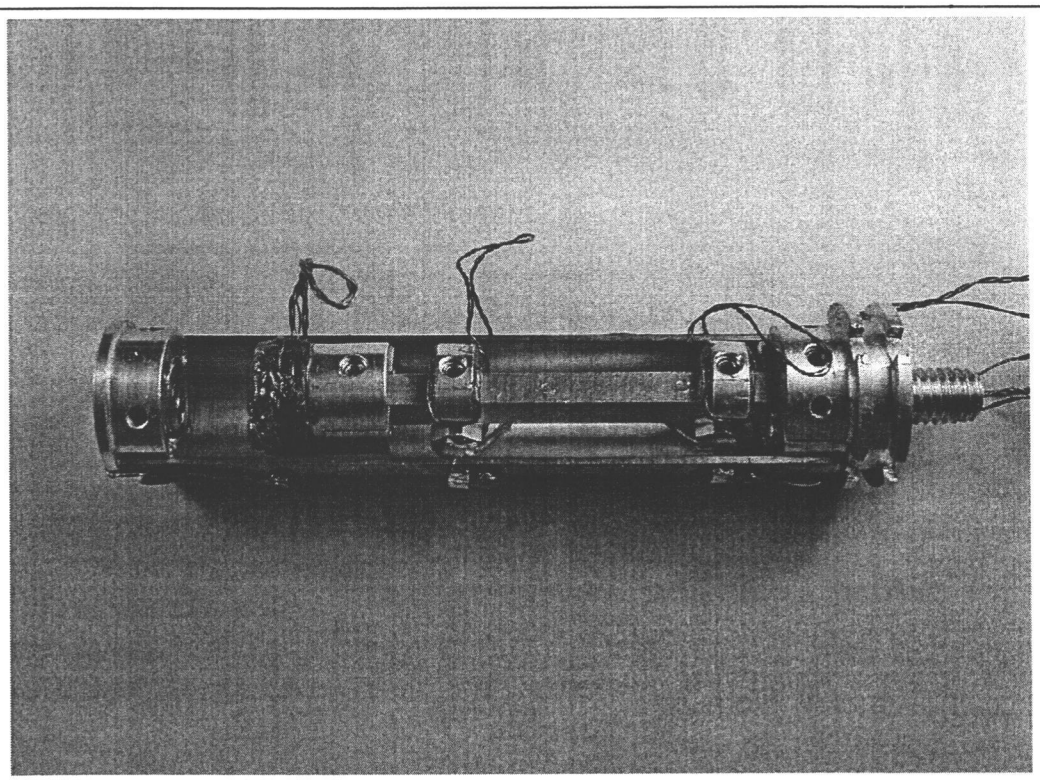

Figure 12. The Routing of Wiring from the Sample to the Radiation Shield.

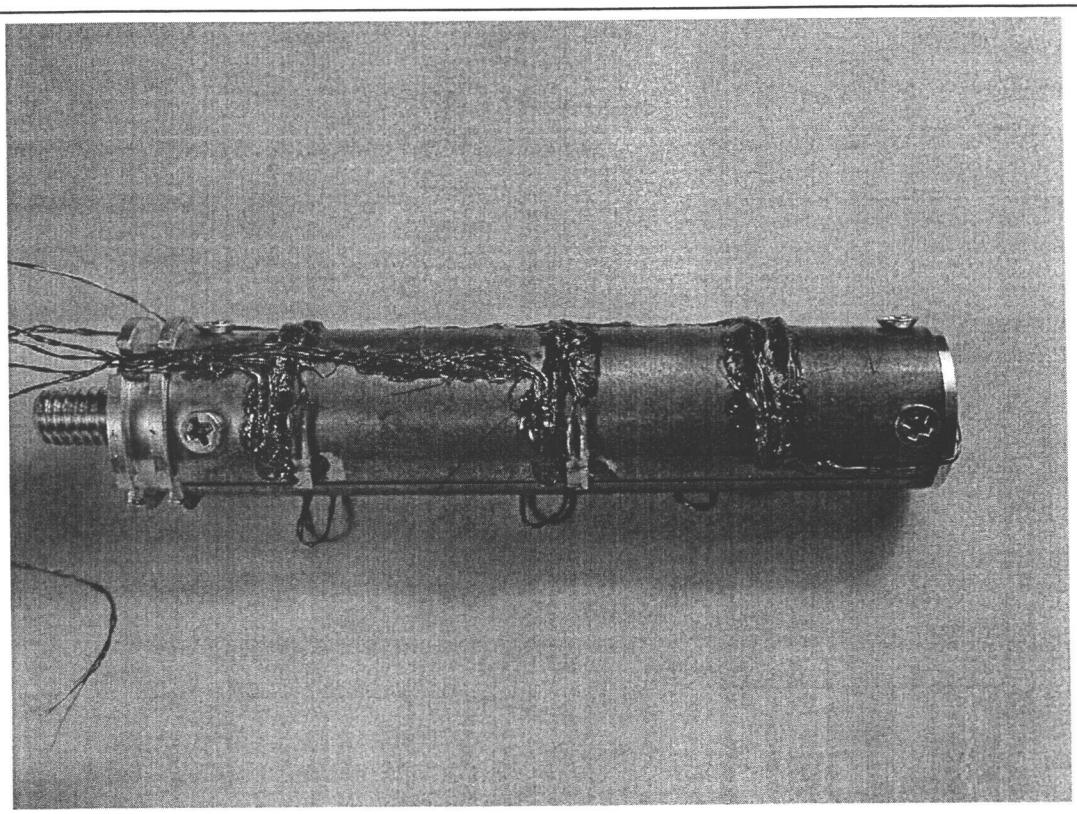

Figure 13. The Routing of Wiring Along the Radiation Shield.

Once assembly of the thermal conductivity test device was completed, the remaining components of the overall system were assembled. First, the test device was attached to the stainless steel probe rod, which had already been wrapped over its length in a single layer of Teflon® tape to prevent electrical shorts between the wires and the rod. The wires were then wrapped along the rod at a rate of approximately once per centimeter of length of the rod to help thermally anchor the wires to its temperature profile. The wrapping was done in a manner such that the wires of each sensor or heater never came in contact with the wires of another component in order to reduce the possibility of electrical shorting from wire to wire. This wrapping of the wires also served to increase the length of the heat conduction path from the thermal conductivity test device to the atmosphere outside the cryostat and therefore reduce the likelihood of a heat leak along the

wires to the test device. The wires were then held firmly in place by the application of a single layer wrap of Teflon® tape over the assembly.

Near the end of the stainless steel probe rod, the wires were routed to pass inside of the hollow rod and run along its axis to exit at its end. At this point the wires were all soldered to the correct pin locations on the back of the three miniature hexagonal electrical connectors that were mounted in the custom fabricated rod end cap. After verifying that the wires were connected correctly and that there were no electrical shorts in the system, the backs of the hex connectors were coated with epoxy to seal the probe rod and therefore allow for the future vacuum pumping of the cryostat sample space.

Having completed the assembly of the thermal conductivity test device and the associated probe test rod, the external system components were produced. The external wiring harness, used to connect the thermal conductivity test probe to the various electronic instruments, was assembled using miniature hexagonal electrical connectors soldered to shielded wire bundles. A flow control valve and associated tubing were then assembled inline with the vacuum pump that would be used to draw the cryogen through the cryostat.

EXPERIMENTAL SETUP

A tremendous number of instruments were required to operate the thermal conductivity test device. Some of these instruments were used to generate and control the test environment, while others were responsible for monitoring or powering the various electrical components of the test device. Most of these systems were then directed from a computer through custom written software. Figure 14 is a schematic of the components and generalized connections that were required to operate the test device. The arrows represent the flow of cryogen and progress from dark to light.

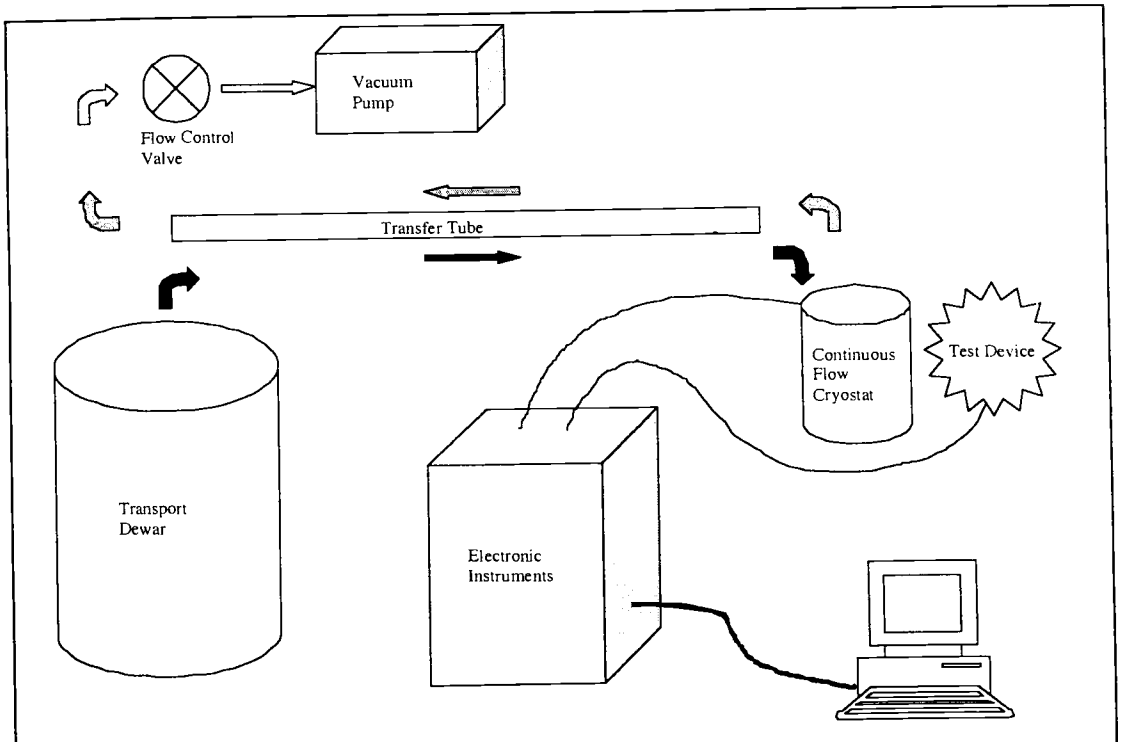

Figure 14. Thermal Conductivity Test System General Diagram.

CRYOSTAT

A continuous flow cryostat, Model CF204 manufactured by Oxford Instruments, was utilized to provide the controlled environment in which the thermal conductivity probe would operate. The inside wall of the cryostat also served as the thermal anchor for the thermal conductivity test device as shown by Fig. 2. A user's manual or specifications sheet did not accompany this donated piece of equipment, so a manual for the most similar instrument that could be located was used to develop a rough understanding of the cryostat. From this basis the instrument was partially disassembled, inspected and repaired, differences with the manual noted, and a new user's manual generated. With increasing experience with the instrument, a revised manual was developed for use.

This particular cryostat used the continuous flow of a cryogen through a sleeve surrounding the sample space to produce the cold test environment. Adjustment of the cryogen flow rate was used to vary the cooling capacity and subsequently the temperature of the sample space. The cooling capacity could also be adjusted through the application of an electrical current to a pair of heating elements connected in parallel and mounted to the cryogen sleeve. A thermocouple was located on the same mounting tab as the heating elements for use in monitoring the temperature of the sample space environment.

TRANSFER TUBE

A vacuum shielded cryogen transfer tube was donated with the cryostat and served to connect the continuous flow cryostat to the cryogen dewar. This instrument was manufactured by Oxford Instruments to mate to the CF204, and as with the cryostat a user's manual was not available. Unfortunately, a manual for a similar transfer tube design also could not be located. As such, the small amount of information relevant to the operation of a transfer tube that was contained in the available cryostat manual was studied and combined with information available in

a text on cryogenic engineering [16] to develop a general understanding of the transfer tube and a procedure for its use.

VACUUM PUMPING SYSTEM

In order to evacuate the cryostat and transfer tube vacuum shields as well as the cryostat sample space, a vacuum pumping system was utilized. The vacuum shields were evacuated by a mechanical pump until a measured pressure of approximately 40 millitorr remained. At that time, a diffusion pump was activated to further reduce the atmospheric pressure in the vacuum shields, to a final value of approximately 10 millitorr. This pumping configuration was left to work on the shields for 12 hours to allow the components to fully outgas. Once the thermal conductivity test device was placed in the cryostat, with the sample installed, the mechanical vacuum pump was used to remove the atmosphere from the sample space.

ELECTRICAL SYSTEMS

Numerous electronic instruments were required for the proper operation of the thermal conductivity test device. These instruments were used to measure the voltages at several locations in the test system, monitor temperature sensors, and operate the various heating elements. These devices were all run simultaneously and controlled by a custom written software program.

Lake Shore DRC-93CA Temperature Controller

This instrument, manufactured by Lake Shore Cryotronics, Inc., is an electronic temperature controller. It was used in this application to monitor the sample temperature sensors and operate the sample heater. The controller operates by taking a user defined target temperature, or set-point, for the selected sensor and applying power to a heating element to bring the sensor up to the desired

temperature. It was configured and directed in its operation by the custom software through the use of a GPIB interface with the computer.

Lake Shore DRC-91C Temperature Controller

The DRC-91C is essentially an older version of the DRC-93CA controller with slightly lower accuracy and a limited remote command capability. Unlike the newer controller, this instrument required the control sensor selection and the calibration curve numbers be manually set on the rear panel through a number of mechanical switches. This controller was used for monitoring the radiation shield temperature sensors and operating the shield heater.

Keithley Model 7001 Switch System

An electronic switch box was utilized to cycle through the three pairs of voltage leads associated with the test system. One voltage pair was measured over the sample heater, a second measured over the calibrated shunt, and the third voltage pair measured the cryostat thermocouple signal. The different wire pairs fed into the Keithley Model 7001 Switch System, which switched from one voltage signal channel to the next when directed by the custom software. The voltage signal from the channel that was currently being monitored was then passed to the digital voltmeter. A low noise, nanovolt (nV) range switch card was utilized for these tests.

Keithley Model 182 Sensitive Digital Voltmeter

The Keithley Model 182 Sensitive Digital Voltmeter was used to measure the voltage signal passed along from the Keithley 7001. The voltmeter was configured for this application with the analog filter turned on, the digital filter set to medium response and activated, and the device set to auto range. It was capable of 1 nV sensitivity on the 3 mV range.

Phillips Model 2831 Programmable Power Supply

Manufactured by Philips, the Model 2831 was utilized as a DC current source for the electrical resistance cryostat heaters. By adjusting the output of this instrument, the cooling capacity within the cryostat and the subsequent sample space temperature could be altered. This instrument was capable of putting out power within the limits of 8 volts and 15 amps, for a total of 120 Watts.

SOFTWARE

In order to automate and properly sequence most of the operation of the thermal conductivity probe and associated electronics, a master control program was created using the National Instruments LabVIEW™ software. Once the control program was started it would guide the user through the test sequence and create a data file to which each data point would be added as it was generated. It also configured the electronic instrumentation to the required settings, verified that the correct circuit boards were installed, and checked that any manual settings for each instrument were correct for the operation of the thermal conductivity test device.

EXPERIMENTAL PROCEDURE

The first step in the preparation of the test system was fairly simple, but quite important to the accuracy of the system. Most of the electronic instrument manuals suggest turning on the device at least an hour prior to testing in order for the circuitry to thermally stabilize and allow the instrument to reach full accuracy. For this application the instruments were turned on the night before the test was to be performed in order to provide approximately 12 hours for the electronics to warm and completely stabilize.

To begin the installation of the material sample in the thermal conductivity test device, the heating element was placed on one end of the sample and attached by tightening the small setscrew. In a similar fashion, the sensor clamps were attached in the proper order and at specific intervals along the length of the sample to ensure that they aligned with the positions of the radiation shield sensors. Next, the sample and attached instrumentation was placed into position in the thermal conductivity test device and the appropriate setscrew tightened. The sample was adjusted so that it ran coaxially with the radiation shield and therefore maintained an even spacing to the shield on all sides. The next task was to carefully route the wires from the sample to the radiation shield through the small wire passages in the shield, then carefully place the second half of the radiation shield into position and install its fasteners. With the excess wire length from the sample instrumentation routed around the outside of the radiation shield along isothermal planes, the test device was wrapped in a layer of Teflon® tape. This was done to hold the excess wire in position and to provide a small level of protection to the wiring and sensors when moving the test probe. Finally, the test probe was very carefully inserted in the sample space of the cryostat and the sealing o-ring nut securely tightened.

Prior to assembly of the remainder of the test apparatus, several of the components of the cryostat system had to be vacuum pumped to ensure that they had not developed leaks that would alter the operation of the system and affect the

test results. This included the transfer tube vacuum shield, the cryostat vacuum shield, and the recently opened sample space of the cryostat. A maximum atmospheric pressure of approximately 30 millitorr remained in the vacuum pumped components during testing.

All of the various electronic instruments were connected next. Custom wire bundles were used to ensure that the thermal conductivity test device was connected properly to the various electronic instruments. The wire bundles were locked in place on the miniature hexagonal electrical connectors of the probe end cap, then the other end of each bundle was attached to the appropriate instruments as shown in Fig. 15. In a similar manner, the wire leads for the continuous flow

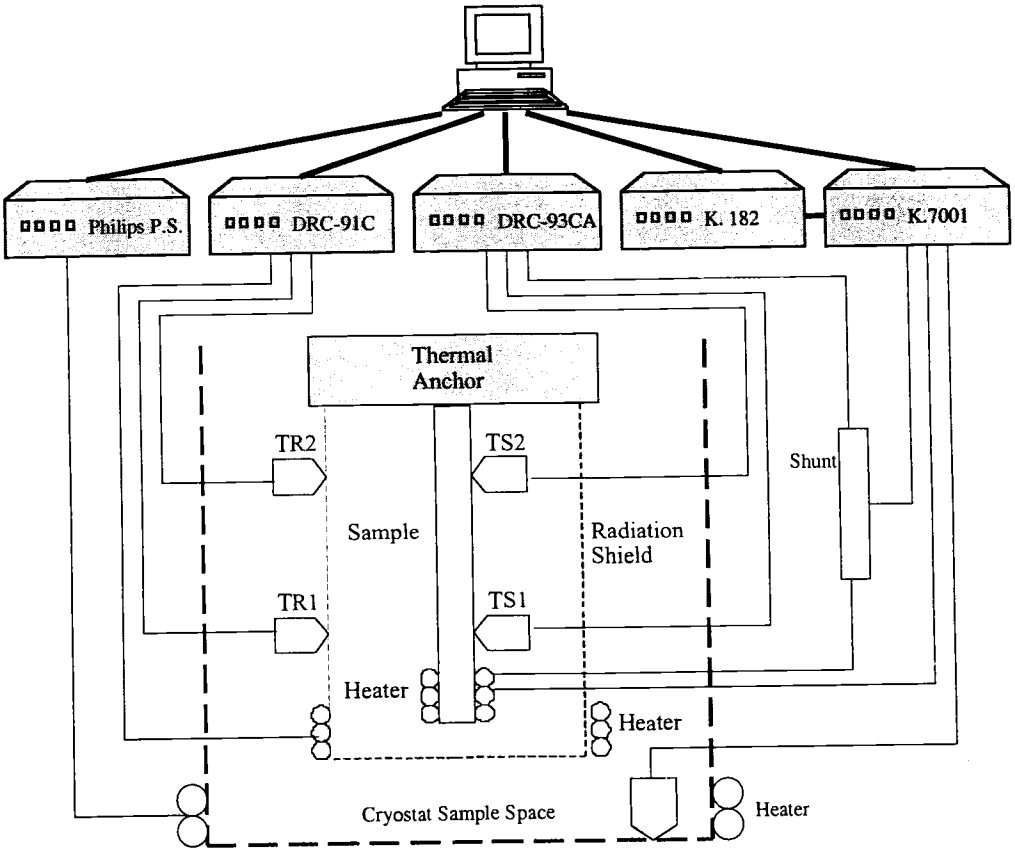

Figure 15. Thermal Conductivity Test System Wiring Diagram.

cryostat were connected to the instrumentation as shown by the wiring schematic of the system.

The next step in preparation for a test run was the assembly of the cryogenic equipment. Liquid helium was the cryogen selected for testing between 4 and 70 Kelvin, and liquid nitrogen was utilized for testing above 70 Kelvin due to its lower cost than liquid helium. For room temperature testing, a coolant was not used. The transfer tube pickup was very slowly lowered into the cryogen dewar to allow the boiled off cryogen time to cool the transfer tube. Once the pickup was fully installed in the dewar, the other end of the transfer tube was slowly, and very carefully, inserted into the mating side arm of the continuous flow cryostat. When the transfer tube and the cryostat were fully pushed together, the coupling nut was tightened. The rubber hose from the transfer tube output was then connected to the cryogen flow control valve, and another hose connected this to the vacuum pumping system. The pump was then turned on and it began to slowly draw cryogen through the system and subsequently cool the cryostat sample space.

A large portion of the control and setup of the thermal conductivity test device and related instrumentation was directed by the custom written software. However, several components required manual adjustment prior to operation of the system. The cryogen flow control valve had to be manually adjusted to set the cooling power of the system. The temperature controller used for the radiation shield needed its control channel set appropriately, and the correct sensor calibration curves assigned.

Once finished assembling the test system, configuring the components, and activating the flow of cryogen through the system, the proper operation of the system was verified. As a first check, the temperatures indicated on the temperature controller front panels were monitored briefly to ensure that they read similar values and were slowly cooling. Next, a monitoring software program was started in order to read all four of the temperature sensors on the thermal conductivity test device and plotted the results as a function of time. After letting

the software run for approximately 15 to 20 minutes, the plot was well developed and the cooling behavior of the system was obvious. Once satisfied that the system was operating correctly, the verification software was stopped.

The next step to make a thermal conductivity measurement was the activation of the software main control program. The front panel of the main program is shown in Fig. 16. Once started, the software directed the user to enter the control parameters in the top left frame of the front panel and click the "System Ready" button when finished. The software waited until the button was activated, then read the control parameters entered on the front panel and used them in the creation of the data file for the test. The default file name was automatically generated from a combination of the sample identification and the date and time listed by the computer. The control parameters and data headings were then added to the file, which was then closed.

Next, the program initialized all of the electronic instrumentation, configured it according to the front panel control parameter inputs, and verified the correct circuit boards were installed and manual switches were set properly. When these tasks were completed the program monitored the four temperature sensors on the thermal conductivity test probe until they were determined to be stable. To do this, 20 measurements of each temperature sensor were made at a brief time delay apart. These measurements were then averaged to create a single temperature point for each sensor that was displayed on the "Temperature Stabilization to Mount Temp." plot of the program front panel. This process was then repeated ten times, with a short delay between each temperature point, to generate a number of points over time. Next, a linear fit to the ten data points for each sensor was performed and 70% of the rise over the fit was then compared to the average standard deviation for the particular sensor. If the rise of the linear fit was less than or equal to the standard deviation, the sensor was considered stable. When all four sensors were found to be stable simultaneously, the program regarded the entire system as

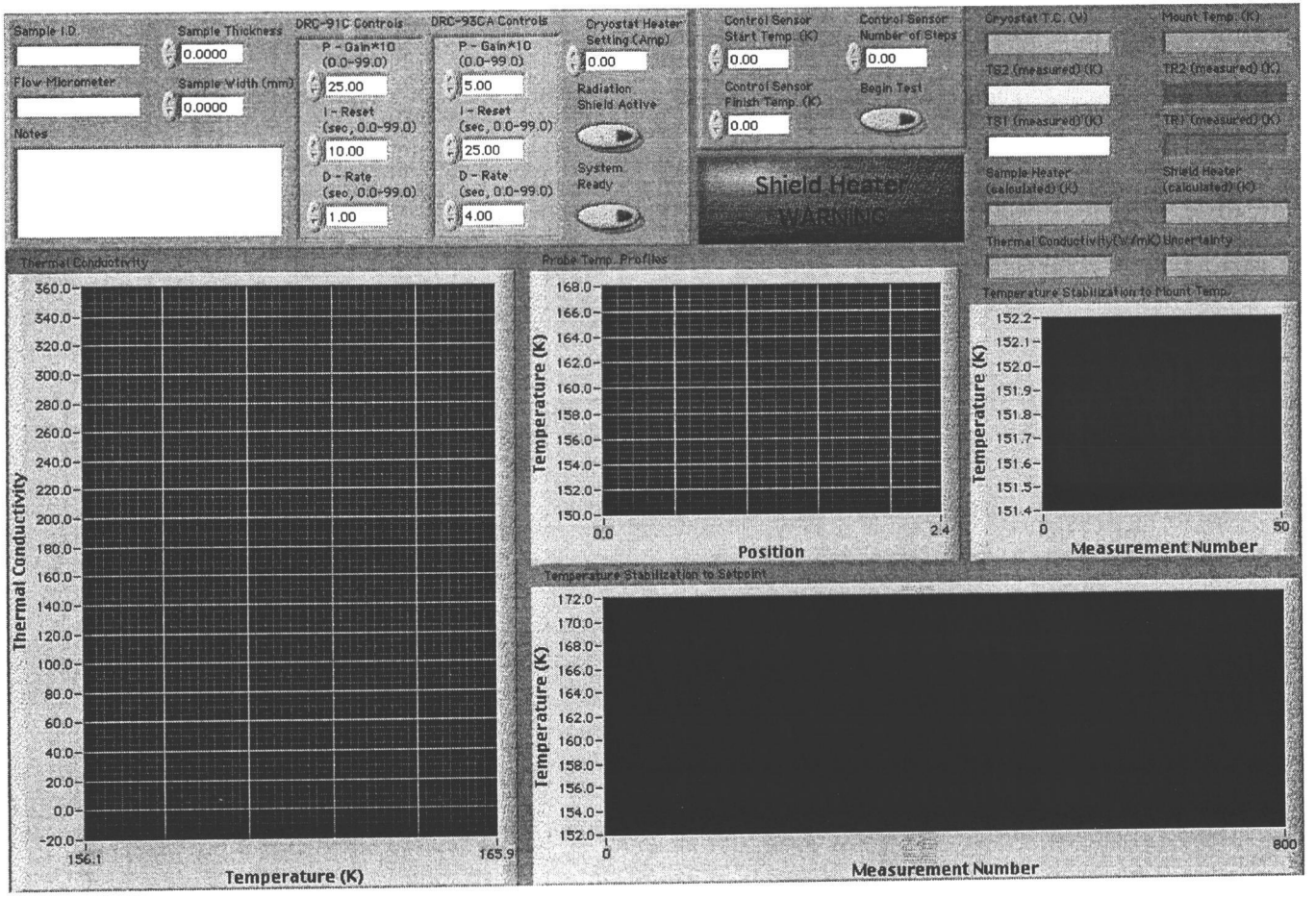

Figure 16. The Front Panel of the Custom LabVIEW Program.

stable. At this point, the program asked the user to confirm or deny the stability of the system.

If the software or the user determined that the sensors were not yet stable, the program would continue to monitor the system. If the user agreed that the system was in fact stabilized, the program calculated the average of the averaged temperature points for each sensor. This value was the temperature of the sample space of the cryostat, with none of the test probe heaters activated, and was subsequently recorded as the mount temperature. The sensor and mount temperatures were then recorded in the previously generated data file and the mount temperature reported to the user.

At this point, the user was directed by the program to enter the necessary setpoint information in the top center frame of the front panel and click the "Begin Test" button when ready. The control sensor start temperature was typically set to approximately three degrees higher than the mount temperature, and the finish temperature and number of steps were selected to produce setpoint increases in increments of two to four degrees. Once the button was activated the program computed the first setpoint and sent it to the temperature controllers, along with heater output ranges.

While the controllers adjusted their heater outputs to bring the sensors at the T1 location up to the first setpoint, the computer program changed to the same kind of monitoring sequence used previously. The setpoint temperature was displayed on the "Temperature Stabilization to Setpoint" plot of the program front panel, along with the current temperatures of the T1 location on the sample and on the radiation shield. The approximate temperature profiles of the sample and radiation shield were simultaneously displayed on the "Probe Temp. Profiles" plot. Once the software determined that the system had stabilized at the first setpoint, the user was asked if they agreed. If not, the program continued to monitor the system. If the user agreed that the system was stable, each of the system measurement was made numerous times and averaged to generate a data point for each measurement. From

these values, the thermal conductivity was calculated and reported at the average of the T1 and T2 temperatures. These values were then displayed on the "Thermal Conductivity" plot of the front panel, and was then recorded to the previously generated file along with all of the other data.

Once the data was recorded, the next setpoint was calculated and assigned to the controllers, and the system began monitoring the temperature sensors for stability. This process was repeated for each setpoint as determined from the previous user inputs to the top center frame of the front panel. When each setpoint had been run and the measurements made and the data saved to the file, the main control program turned off the heater outputs on the temperature controllers as well as the output of the power supply to the cryostat heaters. The user was then informed of the completion of the test series.

This process would generate thermal conductivity data over a small temperature range. As such, the completion of a series of test runs was required at different temperatures to better establish the thermal conductivity of the material as a function of temperature. This entire test sequence was performed twice for a high purity copper sample, twice for a high purity niobium sample, and once for a sample of the bulk metallic glass Vitreloy 1.

RESULTS

Figure 17 is a plot of the accepted and the measured thermal conductivities of the high purity copper sample. The results of the first and second measurement series were plotted separately in conjunction with the accepted thermal conductivity as a function of temperature. This was done to show any variation in the measurement of the thermal conductivity from one test to the next. Measurements were made over the range from 74 to 85 K, from 160 to 166 K, and from 295 to 302 Kelvin.

Figure 18 is a plot of the accepted and the measured thermal conductivities of the high purity niobium sample. The two measurement series were plotted individually, along with the accepted thermal conductivity as a function of temperature. Testing on the niobium sample was performed around 75, 130, and 300 K, as well as around 48 Kelvin.

Figure 19 is a plot of the measured thermal conductivity as a function of temperature of Vitreloy 1 in comparison to high purity niobium, as well as single crystal and amorphous SiO_2. Only a single measurement test run was performed at each temperature range on the Vitreloy 1. These tests were centered at approximately 52, 77, 157, and 296 Kelvin.

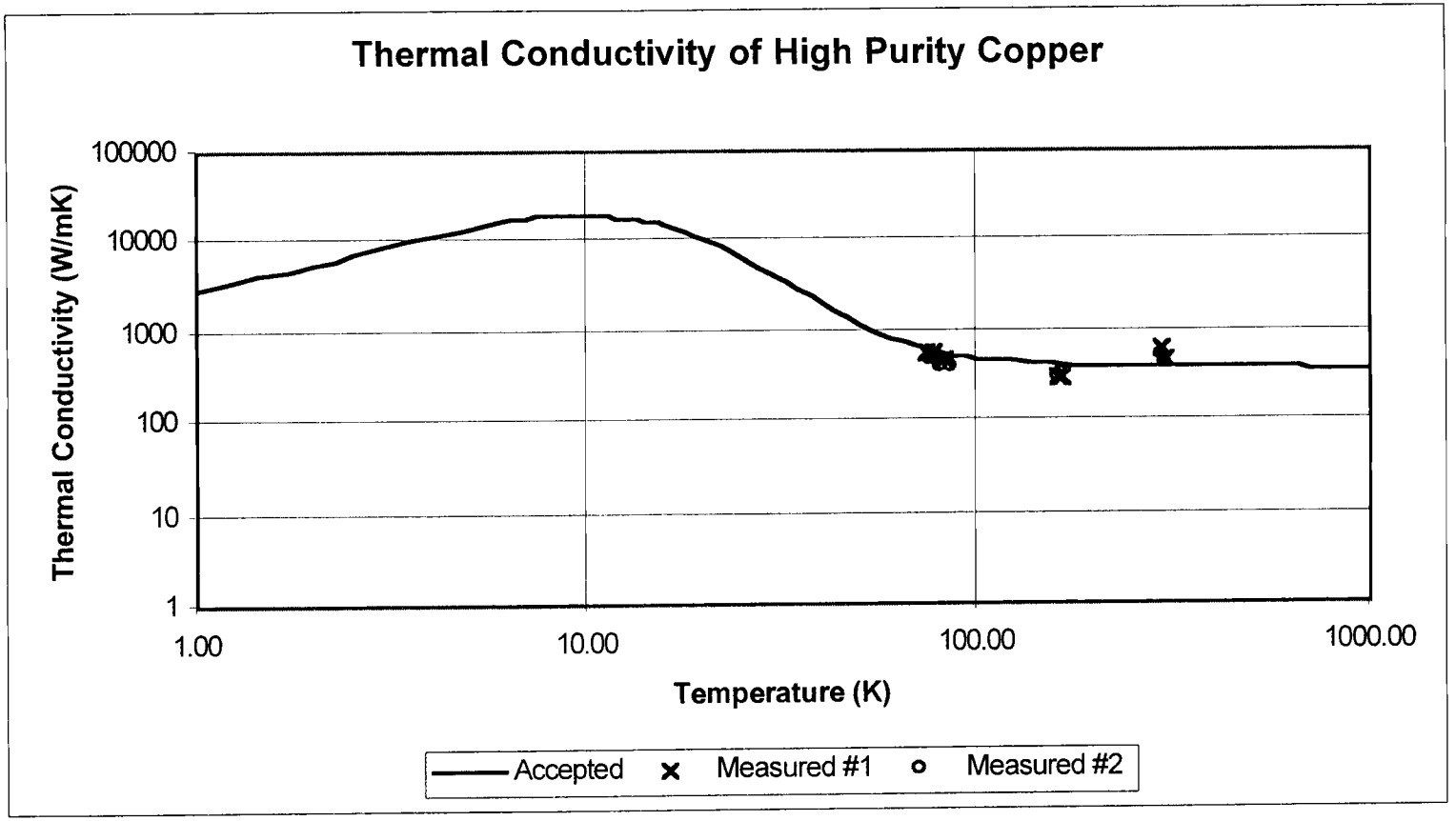

Figure 17. The Measured and Accepted [1] Thermal Conductivities of High Purity Copper.

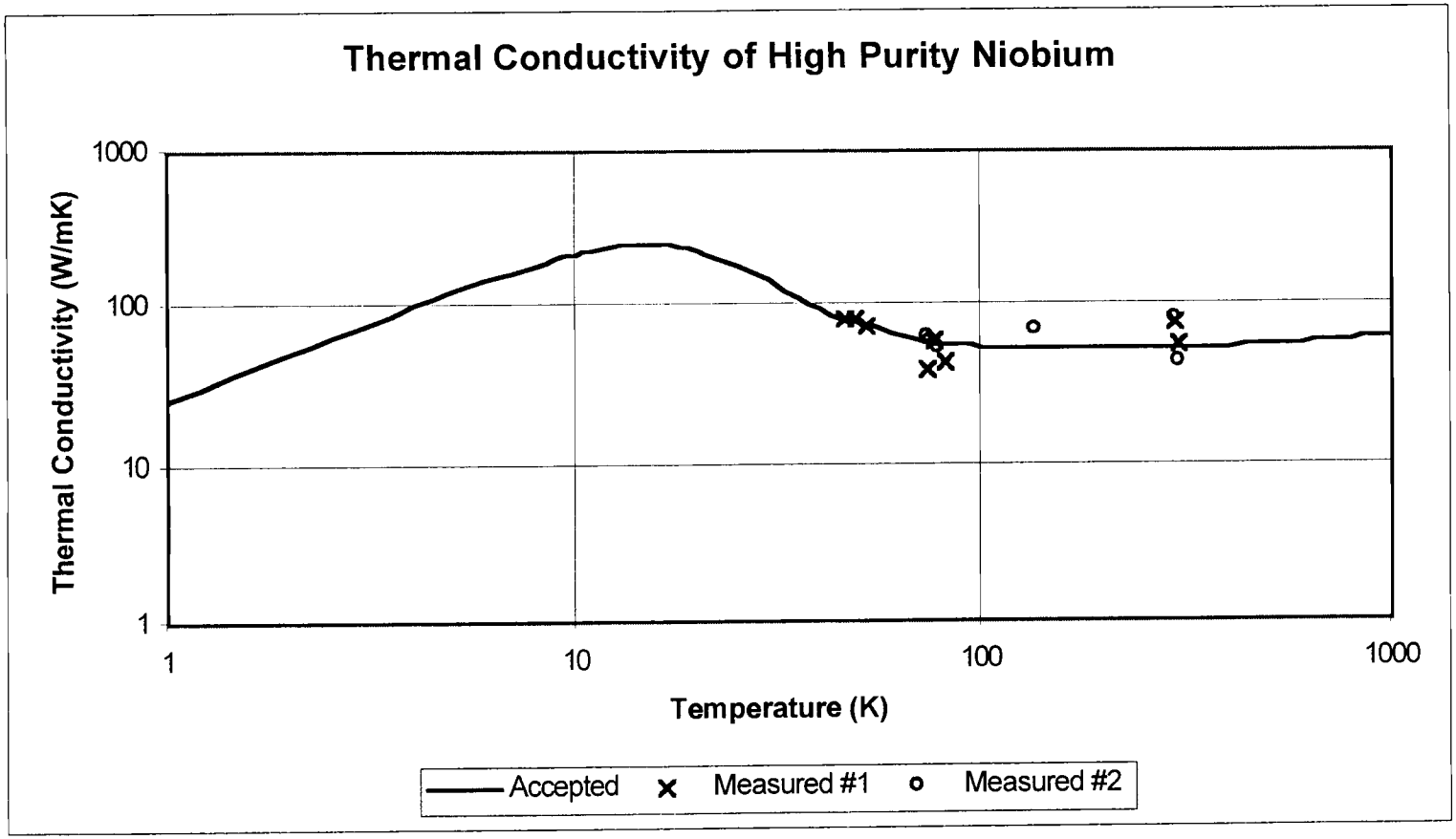

Figure 18. The Measured and Accepted [1] Thermal Conductivities of High Purity Niobium.

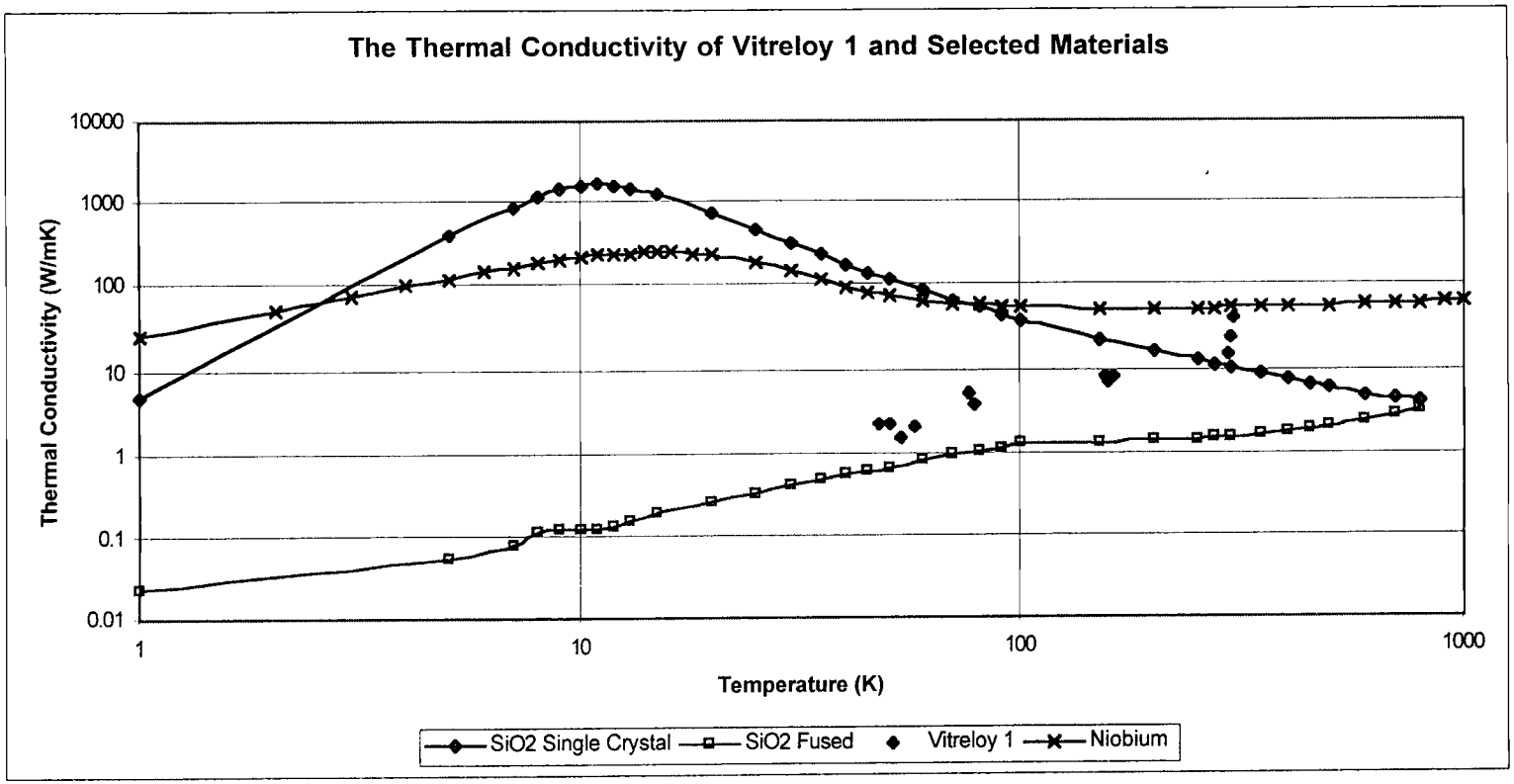

Figure 19. The Measured Thermal Conductivity of Vitreloy 1 in Relation to the Accepted [1] Niobium and SiO_2 Thermal Conductivities.

DISCUSSION

Inspection of Fig. 17 clearly demonstrates the accuracy of the measurement made with the thermal conductivity test device in comparison to the accepted value for a high purity copper sample. The very close grouping of data points from one measurement series to the next highlights the repeatability of the test system over a wide range of temperatures.

The plot of the measured and accepted thermal conductivities of high purity niobium, Fig. 18, show similar results to that achieved with the high purity copper sample. The accuracy and repeatability again appear to be quite good. When combined, the copper and niobium measurements validate the test system over a range of thermal conductivities.

The final plot, Fig. 19, presents the measured thermal conductivity of the bulk metallic glass Vitreloy 1 over the temperature range from 45 to 300 Kelvin. As far as was known, the thermal conductivity of this bulk metallic glass had never been measured at temperatures below 400 Kelvin prior to this project. In the data collected, a general decreasing trend is apparent in the thermal conductivity with decreasing temperature, similar in profile to that seen in the accepted plot of amorphous SiO_2. It is also obvious that the thermal conductivity of Vitreloy 1 over the measured temperature range is greater than for fused SiO_2, due to the free electron contribution of the metal elements to the thermal conductivity. The lack of a uniform crystal structure and the high number of alloying components acting as impurities results in a lower thermal conductivity than for a pure metal, as demonstrated by the poor thermal conductor niobium.

While the data plots look quite good, several things must be kept in mind. First, the thermal conductivity measurements for all three samples at 300 Kelvin are less tightly grouped than at lower temperatures because active cooling was not employed for the room temperature measurements. Instead, the thermal mass of the cryostat was used to provide the thermal anchor, which could slowly warm with

the continued heat input to the thermal conductivity test device. As such, the heat input and the measured temperature difference between the sample temperature sensors could vary as the test progressed.

Next, the calculated uncertainty in the measured thermal conductivity was based upon numerous factors such as geometric, temperature, and electrical measurement errors and their relationships through Eq. 10 [17], and was generally in the range of 10 to 15 percent. However, as stated by Figliola and Beasley [18], "Usually the physical situation is sufficiently complex to preclude the mathematical description of the measurement errors." Some of these unaccounted for errors include the variation in the cross sectional area of the sample over its length, which was particularly apparent in the Vitreloy 1 sample due to the limited accuracy of the special cutting process required to prepare the sample, sensor to sensor temperature differences when the test device was supposedly stable with no heater inputs at a single environmental temperature, and deviations of the sample temperature profile due to connections to the probe itself. It must be understood that the heat flow from the sample to the sensor clamp and temperature sensor generated a deviation from the developed planar temperature profile within the sample [5], with a corresponding uncertainty in the gradient of the sample. A measured temperature error may also occur as a result of the thermal contact resistance over any joints that may occur between the sample and sensor. Also, the accepted thermal conductivity curve [1] for each material given in this paper is for a material with a particular electronic purity as determined by the residual resistivity ratio, or the RRR. The RRR is defined as the ratio of the material's electrical resistivity at 273 Kelvin divided by the resistivity at 4.2 Kelvin. The samples tested here for thermal conductivity were known to be quite pure, but had not been characterized in terms of the RRR and can therefore only be compared in general terms to the published accepted data curves for these same materials. While these potential sources of uncertainty may alter the results, they do not seem to be large enough to bring into doubt the calculated thermal conductivities.

CONCLUSIONS AND RECOMMENDATIONS

It is apparent that the test system developed for this project worked quite well, with the data very closely matching the accepted thermal conductivity curves of the calibration materials over the range of temperatures tested. The system also demonstrated a high level of repeatability in these measurements. The Vitreloy 1 test results, the first known such data for this material, seem logical when compared to known materials. Ideally, more testing should be performed over the entire temperature range on the Vitreloy 1 sample to better establish its thermal conductivity curve. To improve confidence in the thermal conductivity values determined for the Vitreloy 1 sample, tests of the thermal conductivity test device against a low conductivity material with a literature accepted curve should be performed. This would allow for a better check of the accuracy of the system over a larger thermal conductivity range, and more specifically in the range of the unknown material. A more uniform cross section sample of the Vitreloy 1 would also help reduce uncertainty in the calculated thermal conductivity. Also, attempting to get the cryostat to lower temperatures would allow computation of the lower portion of the thermal conductivity curves, where a large rise occurs in the published curves for some materials.

REFERENCES

1. *Thermophysical Properties of Matter: Thermal Conductivity*; Touloukian, Y.S., Ed.; IFI/Plenum: New York, 1970; Vols. 1 and 2.

2. Anderson, A.C. Thermal Conductivity. In *Topics in Current Physics: Amorphous Solids: Low-Temperature Solids*; Phillips, W.A. Ed.; Springer-Verlag; Berlin, 1981; pp 65-78.

3. Dugdale, J. S. *The Electrical Properties of Disordered Metals*; Cambridge University Press; Cambridge, England, 1995; Chapter 1, 2.

4. Johnson, W.L. Bulk Glass-Forming Metallic Alloys: Science and Technology. *MRS Bulletin* **1999**, 24, pp 42-44.

5. Hust, J.G. Thermal Conductivity and Thermal Diffusivity. In *Materials at Low Temperatures*; Reed, R.P., Clark, A.F., Eds.; American Society for Metals: Metals Park, Ohio, 1983; pp 133-161.

6. Speyer, R.F. *Thermal Analysis of Materials*; Marcel Dekker, Inc.: New York, 1994; Chapter 9.

7. Moran, M.J.; Shapiro, H.N. *Fundamentals of Engineering Thermodynamics*, 3rd ed.; John Wiley & Sons, Inc.: New York, 1995; Chapter 2.

8. Callister, W.D. *Materials Science and Engineering: An Introduction*, 4th ed.; John Wiley & Sons, Inc.: New York, 1997; Chapter 6.

9. Incropera, F.P.; DeWitt, D.P. *Fundamentals of Heat and Mass Transfer*, 4th ed.; John Wiley & Sons, Inc.: New York, 1996.

10. *Cryogenic Process Engineering*; Timmerhaus, K.D., Flynn, T.M., Eds.; Plenum Press: New York, 1989.

11. Kittel, C. *Introduction to Solid State Physics*, 7th ed.; John Wiley & Sons, Inc.; New York, 1996; Chapter 6, 17.

12. *Advanced Cryogenics*; Bailey, C.A., Ed.; Plenum Publishing Corporation: New York, 1971.

13. Hammond, C.R. The Elements. In *CRC Handbook of Chemistry and Physics*, 66th ed.; Weast, R.C., Ed.; Chemical Rubber Publishing Company: Boca Raton, Florida, 1986; pp B1-B43.

14. *Machinery's Handbook*, 25th ed.; Green, R.E., Ed.; Industrial Press Inc.: New York, 1996.

15. *Handbook of Applied Thermal Design*; Guyer, E.C., Ed.; McGraw-Hill Book Company: New York, 1989.

16. *Handbook of Cryogenic Engineering*; Weisend II, J.G., Ed.; Taylor and Francis; Philadelphia, 1998.

17. Taylor, J.R. *An Introduction to Error Analysis: The Study of Uncertainties in Physical Measurements*; University Science Books: Mill Valley, CA, 1982.

18. Beasley, D.E.; Figliola, R.S. *Theory and Design for Mechanical Measurements*, 2nd ed.; John Wiley & Sons, Inc.: New York